Probabilistic corrosion hazard maps for reinforced concrete infrastructure in coastal regions

Giuseppe Quaranta[a], Gian Felice Giaccu[b], Bruno Briseghella[c], Camillo Nuti[d]

[a]Department of Structural and Geotechnical Engineering, Sapienza University of Rome, Rome, Italy
[b]Department of Architecture, Design and Urban Planning, University of Sassari, Alghero, Italy
[c]College of Civil Engineering, Fuzhou University, Fuzhou, Fujian, China
[d]Department of Architecture, Roma Tre University, Rome, Italy

ARTICLE HISTORY
Compiled November 18, 2023

ABSTRACT
The development of probabilistic corrosion hazard maps for reinforced concrete infrastructure exposed to airborne chlorides in coastal regions is addressed in the present work, with special attention to bridges. The methodology developed in this study consists of three steps. Initially, spatial distribution, construction year and main features of the existing infrastructure are examined together with the general characteristics of the study area. The second step deals with the elaboration of relevant environmental data, including direction and height of sea waves, sea salinity, temperature, relative humidity, rainfall, speed and direction of wind, and chloride deposition rates. Corrosion hazard maps are obtained next, wherein the corrosion current density is selected as intensity measure. Particularly, they are elaborated for an assigned probability of exceedance given exposure time window and concrete mixture. The presented methodology is applied to develop probabilistic corrosion hazard maps for reinforced concrete bridges exposed to marine atmosphere at Oahu Island (Hawaii, United States). For this case-study, it is also discussed the correlation between the actual condition rating of the existing concrete bridges and the estimated corrosion hazard levels.

KEYWORDS
Bridge; Chloride; Coastal region; Condition rating; Corrosion; Hazard; Pitting corrosion; Reinforced concrete.

1. Introduction

Corrosion is one of the major problems to be addressed towards the proper elaboration and implementation of risk analysis and reduction plans for the built environment. In this context, handling with corrosion phenomena in bridges management policies is especially complicated. To figure out the economic dimension of the existing challenges in this field, it is worth recalling a 2001 report of the Federal Highway Administration (Koch et al., 2001) that has estimated an annual direct cost of corrosion for United States highway bridges equal to 8.3 billion USD (including replacement and maintenance), while a life-cycle analysis has quantified an annual indirect cost to the users

CONTACT Giuseppe Quaranta. Email: giuseppe.quaranta@uniroma1.it

due to traffic delays and lost productivity equal to ten times such value. Furthermore, a recent analysis (ASCE, 2021) regarding the infrastructure in United States has highlighted that 42% of about 617,000 bridges is older than 50 years, and 7.5% of them were classified as structurally deficient. Expenses for bridges in United States were considered inadequate in such analysis, and a required funding for rehabilitation projects equal to 125 billion USD was estimated. It is evident that corrosion is more than a economic concern for bridges management since it can even lead to collapse, possibly in combination with other factors, as demonstrated by recent failures (e.g., Invernizzi et al., 2022; Nuti et al., 2020; Poston & West, 2005). As far as concrete bridges are concerned, carbonation and chloride ingress are among the most common causes that can trigger corrosion of steel reinforcement. The influence of bridges corrosion on the seismic reliability, risk and resilience of transportation networks has been studied by Kurtz et al. (2016), Zanini et al. (2017) and Alipour and Shafei (2016), respectively. Saler et al. (2023) has proposed a procedure to prioritize retrofit interventions on stocks of bridges taking into account seismic vulnerability and corrosion. Recent works by Kashani et al. (2019), Vereecken et al. (2021) and Franceschini et al. (2022) provide a comprehensive overview about corrosion effects in reinforced concrete bridges and pre-stressed/post-tensioned concrete bridges.

Chloride ingress in concrete is usually deemed the most severe cause of corrosion for concrete bridges (e.g., Alipour et al., 2013; Cady & Weyers, 1992; Frangopol et al., 1997; Pelle et al., 2022, 2023; Vu & Stewart, 2000). This deterioration phenomenon is especially relevant for coastal areas, where concrete structures can be continuously subjected to a variety of environmental conditions (viz., tidal, splash and atmospheric zones) that can promote the chloride-induced corrosion of the reinforcement. It should be pointed out that chloride-induced atmospheric corrosion is not the most severe condition for concrete structures in coastal areas (e.g., Bourreau et al., 2020), but it is potentially relevant for a larger number of infrastructure.

The generation of airborne sea salt (i.e., marine aerosol) is a rather complex phenomenon. Briefly, marine aerosol is a cloud of microscopic particles of salt in the air that comes from sea spray formed from breaking surf and ocean whitecaps. The amount of chloride that can be generated at the origin thus depends on sea waves characteristics (Alcántara et al., 2015, 2017) and the concentration of chloride ion dissolved in seawater. On average, sea salinity (i.e., total of all non-carbonate salts dissolved in water) is about 35 g/l in the world's oceans, and the chloride ion concentration is about 19 g/l. However, chloride ion concentration near the coast may vary in time and/or space, for example, because of freshwater outflow, storm drainage, or exploitation of freshwater streams for industrial and domestic uses. The rate at which chloride accumulates on the surfaces in the coastal areas can result significantly altered at sites close to freshwater streams (Guerra et al., 2019). The generated particles of salt are then transported by winds proceeding from sea, and their accumulation into land at large scale commonly depends on shoreline distance (Feliu et al., 1999) and weather conditions (i.e., wind and rainfall) at the site (Corvo et al., 2005; Pham et al., 2019). Marine aerosol particles are usually classified by size, but there is not a general consensus about the dimension thresholds. Ambler and Bain (1955) classified the aerosol particles as "falling particles" and "buoyant particles" if their diameter is larger or smaller than 10 μm, respectively. Particles size determines how long airborne sea salt penetrates: while larger particles are more affected by gravitational settlement, small-sized aerosols can cover long distances inland. Some attempts have been made in the past years to model sea salt transport and deposition in marine atmosphere zones (Cole et al., 2003; Meira et al., 2008).

The potential socio-economic impact of corrosion for bridges exposed to marine atmosphere can be inferred from a recent statistical survey based on almost 20,000 coastal United States bridges by Alogdianakis et al. (2020), who demonstrated that their condition may be affected negatively by sea chlorides at coastal distances up to 2–3 km inland (this evidence emerges from the analysis of bridges in the east coast, and the distance reduces to 1 km for those regions in which deicing salts are also in use). Therefore, the development of corrosion hazard maps for coastal regions can be an important tool for the optimal allocation and prioritization of the resources needed for bridge risk analysis and mitigation through in-situ surveys, structural monitoring, maintenance and retrofitting interventions. According to the United Nations Disaster Relief Organization, hazard mapping can be generally defined as the process of establishing geographically where and to what extent particular phenomenon is likely to pose a threat to people, property, infrastructure and/or economic activities. Corrosion hazard maps can be also employed to support risk management under cascading effects due to other natural hazards that can occur in coastal regions, such as earthquakes (Schexnayder et al., 2014), floods (Qeshta et al., 2019), hurricanes (Padgett et al., 2012), storm surges (Ataei & Padgett, 2015; Contento et al., 2020), tsunami (Fakhruddin et al., 2021; Karafagka et al., 2018), or some combinations thereof (Goda et al., 2021; Ishibashi et al., 2020; Reis et al., 2022; Snaiki et al., 2020).

Territorial studies about the corrosion hazard have been performed for steel structures in South Korea (Kim et al., 2011), Australia and Vietnam (Cole et al., 2012), Thailand (Pongsaksawad et al., 2021), and India (Das & Sarkar, 2021). Corrosion rate (Cole et al., 2012; Kim et al., 2011; Pongsaksawad et al., 2021) and/or corrosivity class (Das & Sarkar, 2021) according to ISO 9223:2012 (ISO, 2012) for steel have been mapped in these researches. Stewart et al. (2011) examined the durability of concrete structures under carbonation- or chloride-induced corrosion for some cities in Australia by accounting for the climate change. Similarly, De Larrard et al. (2014) investigated the durability of concrete structures subjected to carbonation-induced corrosion for some cities in France by taking into account the influence of global warming. Corrosion initiation time (De Larrard et al., 2014; Stewart et al., 2011) and corrosion damage time corresponding to a crack width equal to 1 mm (Stewart et al., 2011) for concrete structures located in different cities have been considered in these researches.

Within this framework, the novel contribution of the present paper is a rational and comprehensive methodology towards the development of probabilistic corrosion hazard maps at regional scale for reinforced concrete infrastructure exposed to marine atmosphere in coastal areas. The implemented approach mainly consists of three phases. Spatial distribution, construction year and typology of the reinforced concrete structures exposed to corrosive agents are first examined. Next, relevant environmental data are elaborated. The probabilistic corrosion hazard maps are obtained later on: they provide the spatial distribution of the selected corrosion intensity measure for an assigned probability of exceedance given the exposure time window and the concrete mixture. After a general outline of the proposed procedure in Section 2, the methodology is thoroughly presented from Section 3 to Section 5 along with its application to the selected case-study, namely Oahu Island (Hawaii, United States). It is believed that this can facilitate its logical presentation and, ultimately, is useful for better explaining the various steps as well as the underlying assumptions and motivations. Section 6 includes a sensitivity analysis and a critical discussion about the possible correlation between the estimated corrosion hazard levels and the actual condition rating of the existing concrete bridges over the study area. Although the development of probabilistic corrosion hazard maps is illustrated with reference to a specific case-study,

the implemented methodology has a broad validity and can be adapted to assess the chloride-induced corrosion hazard for general reinforced concrete structures located in other coastal regions. Some conclusive remarks about the proposed approach and its implementation to other study areas are provided in Section 7.

2. Outline of the methodology for mapping the corrosion hazard

The general aim of the present contribution is framed in the context of the performance-based engineering. In a broad sense, it is "based on the premise that performance can be predicted and evaluated with confidence in order to make, together with the client, intelligent and informed tradeoffs based on life-cycle considerations rather than construction costs alone" (Lee & Billington, 2009). Performance-based engineering rests on a methodology that consists of four steps, namely hazard analysis, structural analysis, damage analysis, and loss analysis (Lee & Billington, 2009). The entire procedure must be conducted in a probabilistic manner, such that the inherent variability and the involved uncertainties can be properly incorporated. This concept has been implemented in the past years to cope with the assessment of structures exposed to different natural hazards, such seismic hazard (e.g., Bertero & Bertero, 2002; Günay & Mosalam, 2013; Porter, 2003) and wind hazard (e.g., Ciampoli et al., 2011; Griffis et al., 2013; Spence & Arunachalam, 2022). The extension of the performance-based engineering framework to durability issues related to corrosion phenomena in reinforced concrete structures is thus explored in the present work, with focus on hazard analysis.

In this regard, the development of chloride-induced probabilistic corrosion hazard maps for reinforced concrete bridges in coastal regions exposed to marine atmosphere is here addressed. The general workflow implemented for this task encompasses three main steps.

- Initially, data mining stage is focused on the characteristics of the study area. The collection of data about the geometry and the orography of the study area is needed to reconstruct next the spatial variation of some environmental variables. The potential impact of the corrosion on the targeted infrastructure stock (e.g., bridges) within the study area should be also discussed by examining relevant data. Construction type, number, position with respect to the shoreline, age, construction system and building materials are useful information to infer the relevance of corrosion phenomena due to the exposure to marine atmosphere. Plans for extending the lifetime of existing structures are also important since they can urge the elaboration of corrosion hazard scenarios and can dictate the selection of the time window. Critical facilities mapping also helps to improve communications among participants in the hazard management process and between planners and decision-makers.
- The second step is concerned with the analysis of the exposure conditions in the study area. This requires the collection and analysis of environmental data pertinent to chloride-induced corrosion phenomena due to marine aerosol, such as direction and height of sea waves, sea salinity, temperature, humidity, rainfall, speed and direction of wind, and chloride deposition rate. Corrosion hazard mapping calls for the estimation of the spatial variation of several environmental variables. A data-driven approach can be implemented if enough data are available, while a physics-based model must be adopted otherwise. The analysis of

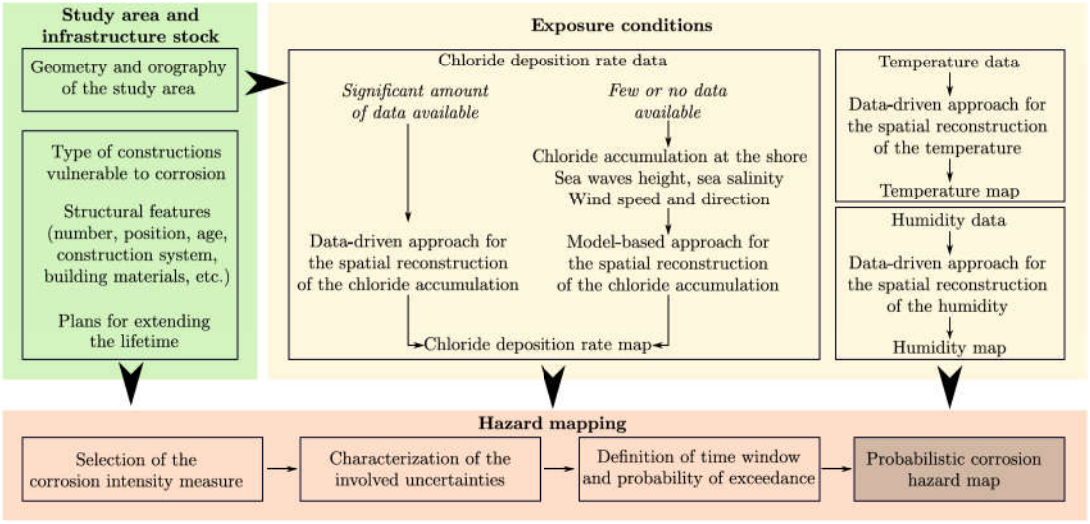

Figure 1. Workflow of the proposed methodology for the development of chloride-induced probabilistic corrosion hazard maps for reinforced concrete structures in coastal regions exposed to marine atmosphere.

the exposure conditions is also important for a comprehensive understanding of the environment influence on the corrosion hazard (Alcántara et al., 2015).

- Chloride-induced corrosion hazard maps are then elaborated in the last stage. To this end, the intensity measure that serves at quantifying the hazard must be specified. The selected intensity measure is thus evaluated over the study area taking into account the involved uncertainties. Therefore, once the time window and the probability of exceedance are assigned, corrosion hazard maps are elaborated also accounting for the concrete mixture.

The workflow of the proposed methodology for mapping the corrosion hazard at regional scale due to the exposure to marine atmosphere is shown in Figure 1. As far as the spatial reconstruction of the exposure conditions is concerned, a data-driven approach is here intended as a way to estimate the spatial distribution of the field variable starting from a discrete set of data without direct modeling of the underlying phenomenon. In general, this can be done by means of deterministic methods (e.g., nearest neighbours, inverse distance weighting) or geostatistical methods (e.g., kriging, cokriging) (Li & Heap, 2008). Alternatively, a model-based approach can be adopted. Differently from a data-driven approach, the spatial distribution of the field variable in such case is obtained from a suitable physics-based model able to simulate the underlying phenomenon. In most applications, a large amount of temperature and humidity data is often available, and thus a data-driven approach can be adopted to estimate their variability over the considered study area. Conversely, a data-driven approach can be implemented to estimate the spatial reconstruction of the chloride accumulation inland in some cases only, because no or limited measurements are available most of the time. In such circumstances, a physics-based model can be adopted starting from a few common data (e.g., sparse measurements of the chloride deposition rate at the shore or indirect estimates based on empirical relationships with the sea wave height, together with data about wind speed and direction). All the steps involved in the proposed methodology will be thoroughly discussed henceforth along the application to the selected case-study.

3. Study area and infrastructure stock

The selected case-study is Oahu Island, which is the third-largest of the Hawaiian Islands in United States. Oahu Island is about 71 km long and 48 km across, while its area and shoreline length are about 1,545 km^2 and 365 km, respectively. The study area is shown in Figure 2, where the geodata employed for plotting the coastline are retrieved from the State of Hawaii's Open Data[1] web portal. Elevation contours with a constant step equal to 152.4 m are also superimposed to the island map in Figure 2. Geodata for plotting the elevation contours are retrieved from the Hawaii Statewide GIS Program[2] website.

In the present work, special attention is paid on the chloride-induced corrosion hazard for bridges located within the study area. In this regard, Figure 2 also provides an overview about spatial distribution and construction year of reinforced concrete, pre-stressed/post-tensioned concrete bridges and steel bridges (bridges age in Figure 2 are calculated with respect to 2022). Position, construction type and year built are retrieved once again from the State of Hawaii's Open Data web portal, which refers to the National Bridge Inventory for Hawaii (as of December, 2020).

Overall, bridges data in Figure 2 motivate the elaboration of chloride-induced corrosion hazard maps for the selected study area. In fact, since the largest part of the major transportation network develops along the island border, several bridges are rather close to the shoreline, which can facilitate the deposition of a significant amount of sea chlorides on their surfaces. More precisely, since most of the bridges are placed at a coast distance less than 3 km, this implies that the condition of most existing bridges may depend on the exposure to sea chlorides according to the macroscopic statistical study by Alogdianakis et al. (2020). Moreover, it can be inferred from Figure 2 that most of the bridges are more than 50-years old. The impact of chloride-induced corrosion is especially relevant for concrete bridges (i.e., reinforced concrete and pre-stressed/post-tensioned concrete bridges) because they are many more than steel bridges, as shown in Figure 2. Hence, it seems appropriate to pay attention on the chloride-induced corrosion hazard for the concrete bridges within the study area. Particularly, the average age for concrete bridges in Oahu Island (referred to 2020) is about 58 years, in line with the Hawaii's average bridges age equal to 60 years and larger than the nation's average bridges age equal to 43 years (ASCE, 2019). Since it is generally recognized that corrosion initiation for concrete structures lasts from 15 to 30 years while corrosion effects start to be visible between 25 and 40 years after construction (Nuti et al., 2020), concrete bridges in the study area are likely experiencing or may experience in the short/mid-term the effects due to corrosion. It is noted that most bridges in Hawaii's inventory were typically designed for a 50-year service life (ASCE, 2019).

The elaboration of corrosion hazard scenarios might be also a useful support for ongoing bridges management policy in the study area. In fact, with the large number of old bridges in Hawaii, state and counties implement repairs and rehabilitation to try to extend the service life of bridges as much as possible because replacement projects are expensive (e.g., the estimated unit cost for bridge replacement is 7,255-8,471 USD/m^2) and usually challenging (ASCE, 2019).

[1] Webpage: `https://opendata.hawaii.gov/`.

[2] Webpage: `https://geoportal.hawaii.gov/`.

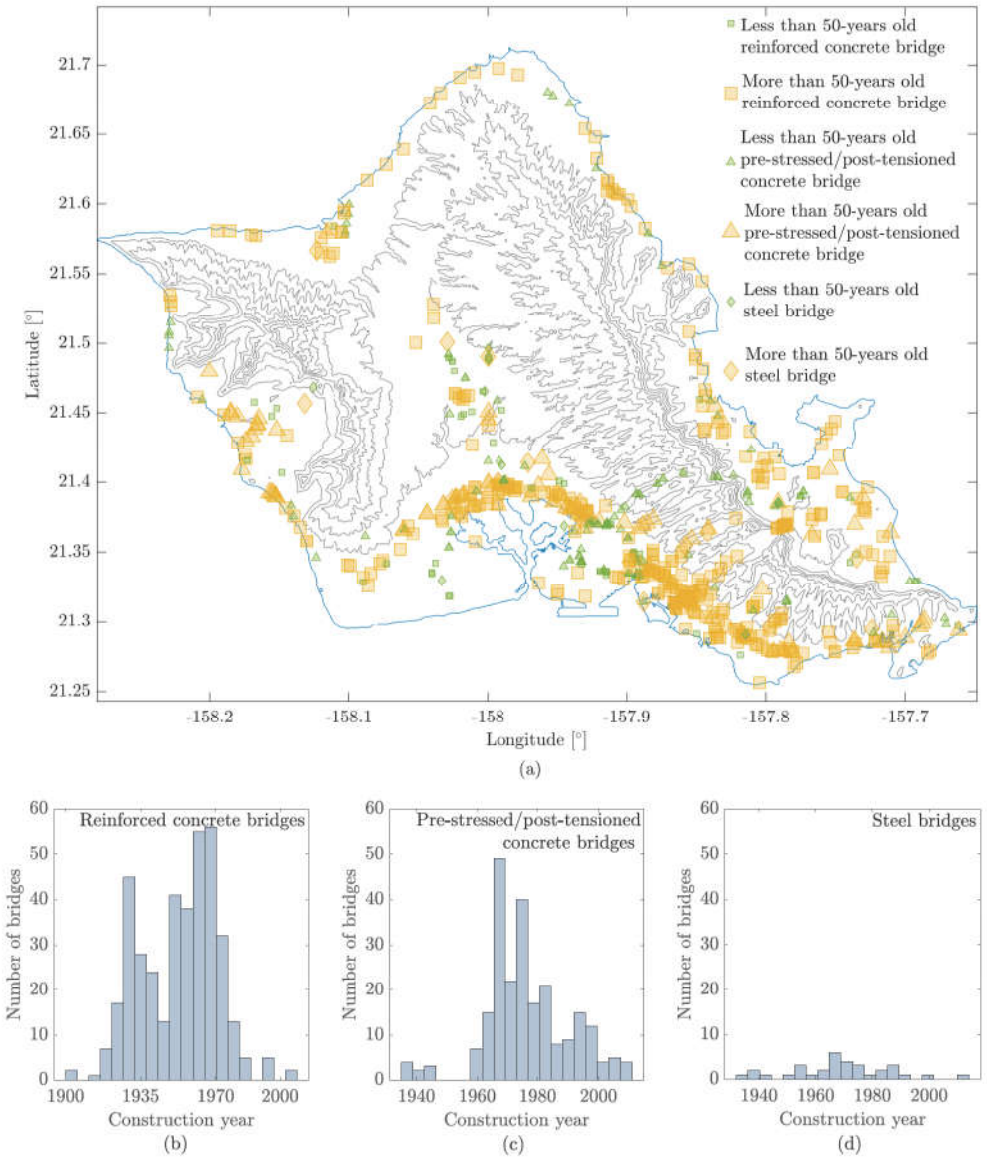

Figure 2. Map of the study area with number, location and age of existing bridges (a), together with construction year of reinforced concrete bridges (b), pre-stressed/post-tensioned concrete bridges (c) and steel bridges (d).

4. Exposure conditions

4.1. Sea waves and salinity

Figure 3 reports data about sea waves and salinity. These data are collected from the Pacific Island Ocean Observing System[3]. For some representative buoys, Figure 3 provides data about wave height (i.e., vertical distance of a sea surface wave from trough to crest, in terms of significant wave height) and peak wave direction (i.e., direction in which the dominant, or peak, sea surface waves are traveling from). Selected buoys measure waves 1.6-6 km offshore and are moored in water 35-291 m deep. Data about sea waves refer to 1-year period starting from April, 2020. Sea salinity data are elaborated considering all the three buoys for which the information is available. Selected buoys measure salinity 0.3-1.6 km offshore and are moored in water 0.3-9 m deep. Salinity data in Fig. 3 approximately cover the period 2008-2011. Indeed, an almost complete set of simultaneous salinity measurements is available for all the buoys between 2008 and 2011 whereas no data is available before 2008 and a significant amount of data is missing for at least one buoy as of 2012.

It can be inferred from Figure 3 that the significant wave height values at Ohau Island mostly range between 1 m and 4 m on the easter and northern coast. Here, the wave height varies seasonally with the intensity of the trade winds. Northwest shores are exposed to relatively larger swells from storms in the western north Pacific. The largest values of the significant wave height are observed in the north shore, where it is sometimes larger than 5 m. South shores receive smaller swells from southern hemisphere storms, and the significant wave heights are mostly between 1 m and 3 m. The minimum and maximum average significant wave heights recorded at the buoys shown in Figure 3 are equal to 0.85 m (buoy at the Pearl Harbor Entrance) and 1.68 m (buoy at the Kāneʻohe Bay), respectively. These wave height values can possibly produce a non negligible accumulation of chlorides inland according to previous measurements in Spain (Alcántara et al., 2015; Feliu et al., 2001).

It can be observed from Figure 3 that sea salinity near the coast can be subjected to spatial and/or temporal fluctuations. Sea salinity at Ala Wai buoy is slightly lower than that recorded at the two other buoys. Therein, the median value of the sea salinity is lower than 35 PSU while larger median values have been found for the other two buoys. In this regard, it is useful to recall that salinity values below 35 PSU near the coast may be due to fresh water outflow and storm drainage. In the present case, this may be due to the Ala Wai Canal, which drains the watershed encompassing Mānoa and Pālolo Valleys and empties into the ocean close to such buoy. Anyway, it is evident that such variations of the sea salinity can somehow affect the distribution of the chloride deposition rates inland, since they influence the amount of salt generated by breaking waves.

4.2. Wind, temperature, relative humidity and rainfall

Data about wind speed and direction recorded at some representative stations are plotted in Figure 4 whereas some wind maps for the study area are given in Figure 5. Wind roses and maps in Figure 4 and Figure 5 are elaborated on average daily values. Wind data for this study are retrieved from the RAWS USA Climate Archive[4] and the

[3]Webpage: `https://www.pacioos.hawaii.edu/`.

[4]Webpage: `https://raws.dri.edu/`.

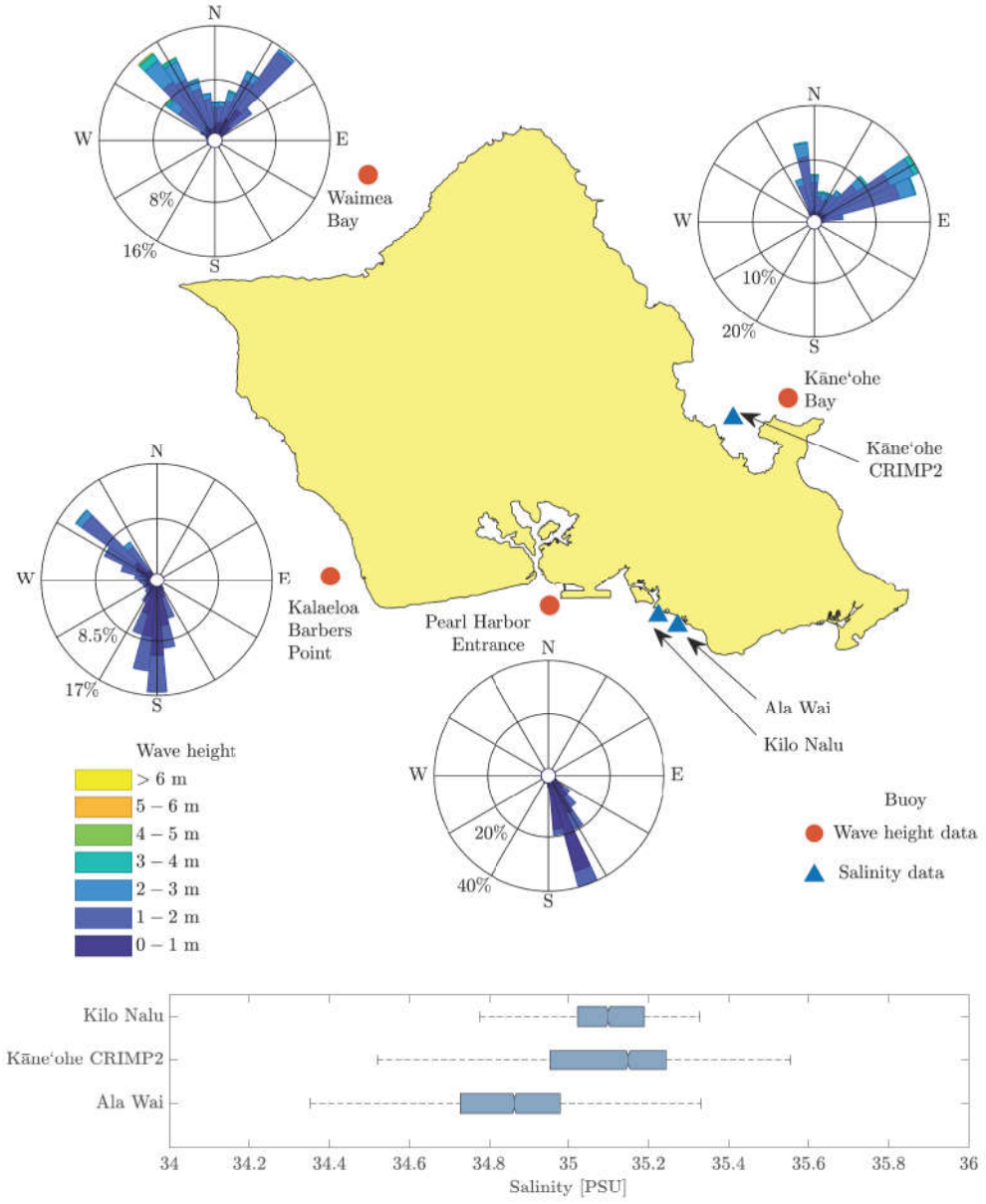

Figure 3. Height and direction of sea waves, together with sea salinity data.

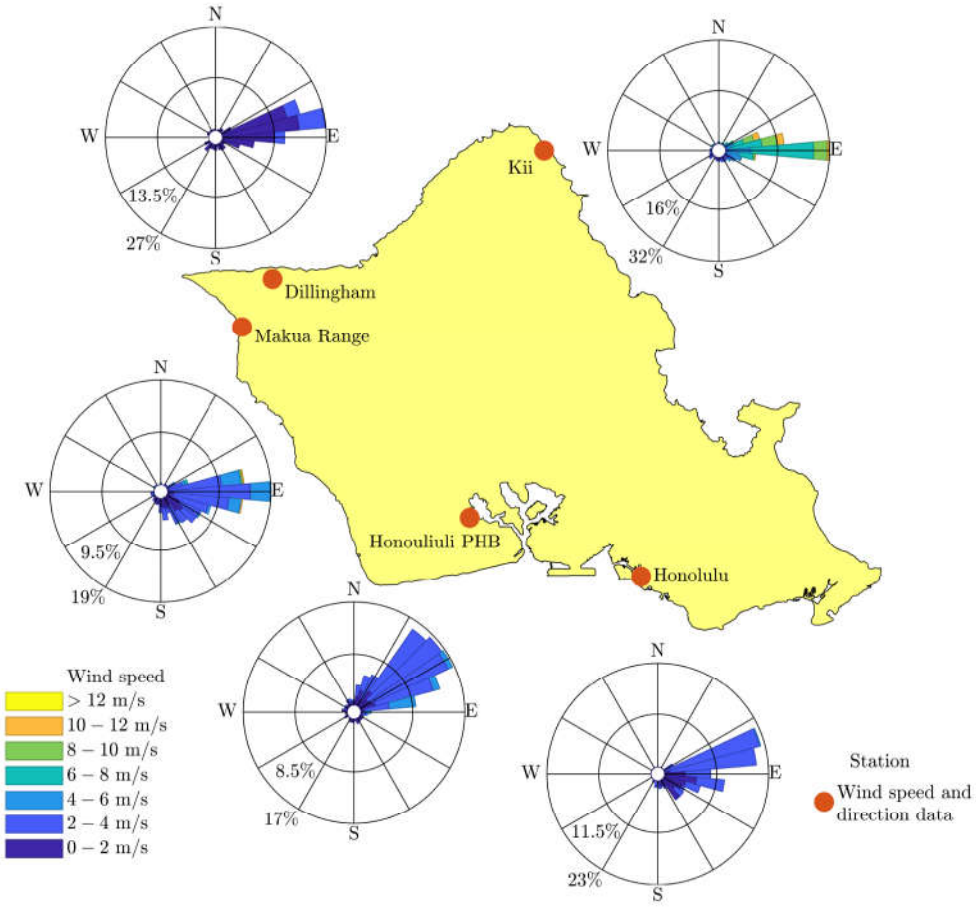

Figure 4. Wind mean speed and direction for some stations.

National Oceanic and Atmospheric Administration[5]. They span over one year, that is 2020. The elaboration of daily wind maps in Figure 5 rests on data collected from 16 wind stations scattered throughout the island. The altitude of the selected wind stations ranges between 1.52 m and 722.38 m. The daily average wind velocity field is estimated by nonlinear spatial interpolation on the basis of the wind data retrieved from the available stations. The orography of the island is thus implicitly considered in the interpolation, and the maps in Figure 5 ultimately provide daily average wind speed and direction close to the ground. The wind velocity field is evaluated by vector analysis in order to obtain the averaged wind properties for each day of the year according to the approach illustrated by Grange (2014). Scattered wind data throughout the island are interporlated by means of biharmonic spline.

Trade winds blowing from east to west are the most common winds, as it can be inferred from Figure 4 and Figure 5. Therefore, considering the prevailing wind conditions, the east coast is windward while the west coast is leeward. While trade winds prevail more than 90% of the time in the summer and sometimes persisting for almost an entire month, they may occur only 40% to 60% of the time in the winter. Sometimes, the wind blows over the island from south-west (this is also known as Kona wind), as it can be observed in Figure 5. However, Kona winds usually don't last for more than a day. The maximum values of the wind speed are frequently recorded in

[5]Webpage: `https://www.noaa.gov/`.

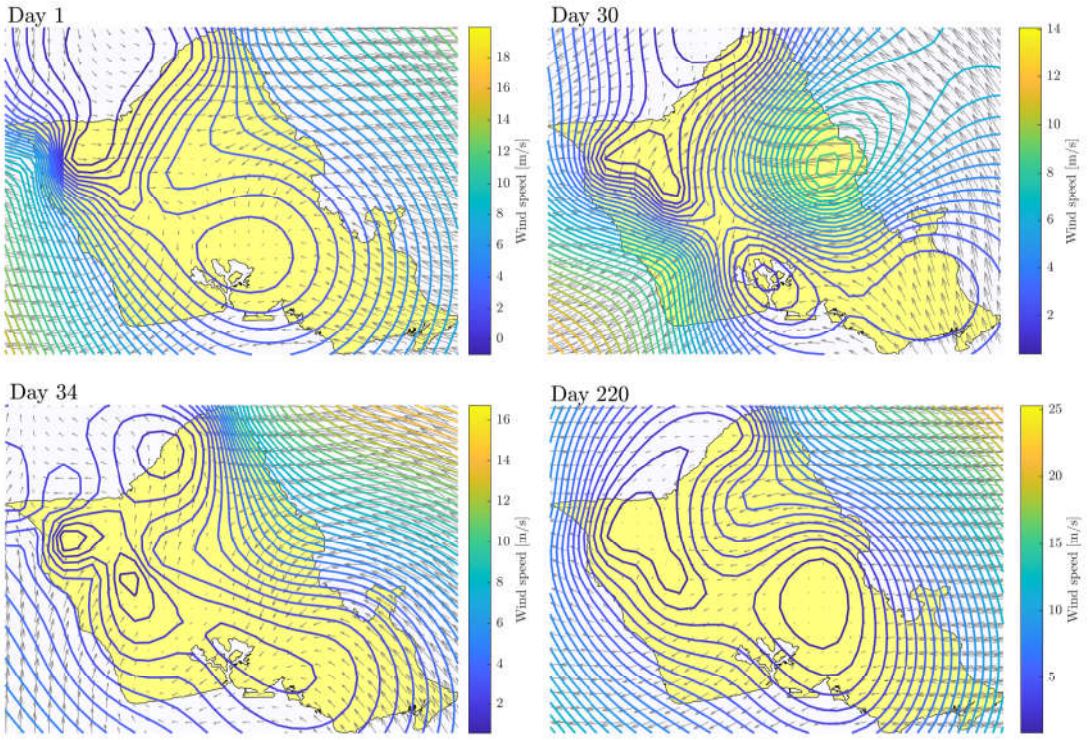

Figure 5. Some daily wind maps obtained by means of spatial interpolation of the data collected from the available stations.

the northern part of the east coast, as shown in Figure 4. Here, the average annual wind speed is around 6 m/s, whereas it mostly ranges between 1 m/s and 3 m/s in the remaining zones of the island. Overall, the wind pattern is thus expected to promote the chloride accumulation inland mainly on east and west sides of the island. A deeper penetration inland is reasonably expected in the northern part of the east coast because of the higher wind speed that blows in such zone of the island.

According to ANSI/ASHRAE Standard 169 (ANSI/ASHRAE, 2013), climate at Hawaii Islands is very hot and humid (climate zone 1A). The maps about surface temperature and relative humidity in the study area are part of 2014 Climate of Hawaii project (Giambelluca et al., 2014). Rainfall data are reported by Giambelluca et al. (2013). Average annual values of surface temperature, relative humidity and rainfall are mapped into Figure 6.

High and low values of temperature and humidity occur in different areas of the island. Highest temperatures are found along the shoreline, where average values close to 28 °C are observed. Herein, the humidity rate is minimum, about 70%. The opposite holds true when moving away from the coast. Inland average temperature and humidity rate values reach approximately 16 °C and 85%, respectively. It is evident that the spatial distributions of temperature and humidity conflict each other in ruling the corrosion hazard level for concrete structures at territorial scale, since it amplifies when both temperature and humidity increase.

Rainfall distribution is highly asymmetric in both time and space. Amounts are greatest on windward and least on leeward. Leeward zones and other dry areas obtain their rainfall mainly from a few winter storms. Here, rainfall is usually seasonal and summers are dry. In the wetter regions, rainfall comes from both winter storms and

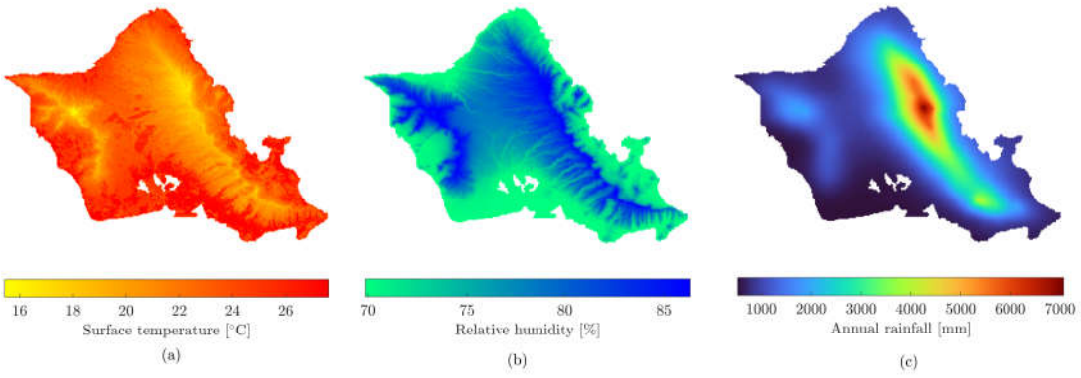

Figure 6. Average annual values of surface temperature (a), relative humidity (b) and rainfall (c).

trade wind showers, and seasonal differences are much smaller. Hence, rainfall are less frequent on leeward and more regularly distributed over the year on windward. This implies that the rainfall distribution conflicts with the pattern of the inland chloride deposition promoted by the prevailing wind regime. In fact, while inland penetration of chlorides is facilitated on windward, the small seasonal differences of the rainfall distribution in this zone is more effective in reducing the amount of chlorides that can deposit on the structures. Conversely, a reduced inland penetration of chlorides is expected on leeward, but the low level of occasional rainfall in this zone facilitates their accumulation.

The potential effects of climate change on chloride-induced corrosion hazard for coastal areas should be also discussed. Some studies by Bastidas-Arteaga et al. (2010) and X. Wang et al. (2012) suggest that this effect may be rather low. Particularly, X. Wang et al. (2012) found that chloride-induced corrosion is less sensitive to global warming than carbonation-induced corrosion, and relate the low impact to the fact that temperature rise near the coast (i.e., where airborne chloride accumulates easily) is expected to be less marked than that occurring inland (i.e., where airborne chloride concentration is low or null). Bastidas-Arteaga et al. (2013) also pointed out that global warming has more influence where humidity and temperature are subjected to large seasonal variations. This condition, however, does not apply for the study area since temperature and humidity do not exhibit large seasonal fluctuations throughout the year. Considering the available findings, the effect of climate change will be not taken into account in the elaboration of the hazard maps, but this issue certainly deserves ad hoc investigations in future works.

4.3. Chloride deposition rate

Chloride deposition rates employed for the considered study area are taken from the technical report by Suzuki and Robertson (2011), in which data for 126 testing sites are provided. The map of the chloride deposition rates for all testing sites is illustrated in Figure 7.

The spatial distribution of the chloride deposition rates reported by Suzuki and Robertson (2011) is highly variable, with a maximum value equal to 347.54 $mg/m^2/day$ while mean and standard deviation are equal to 38.92 $mg/m^2/day$ and 56.37 $mg/m^2/day$, respectively. While the chloride deposition rate at mid-large scale basically depends on shoreline distance and environmental conditions, local factors

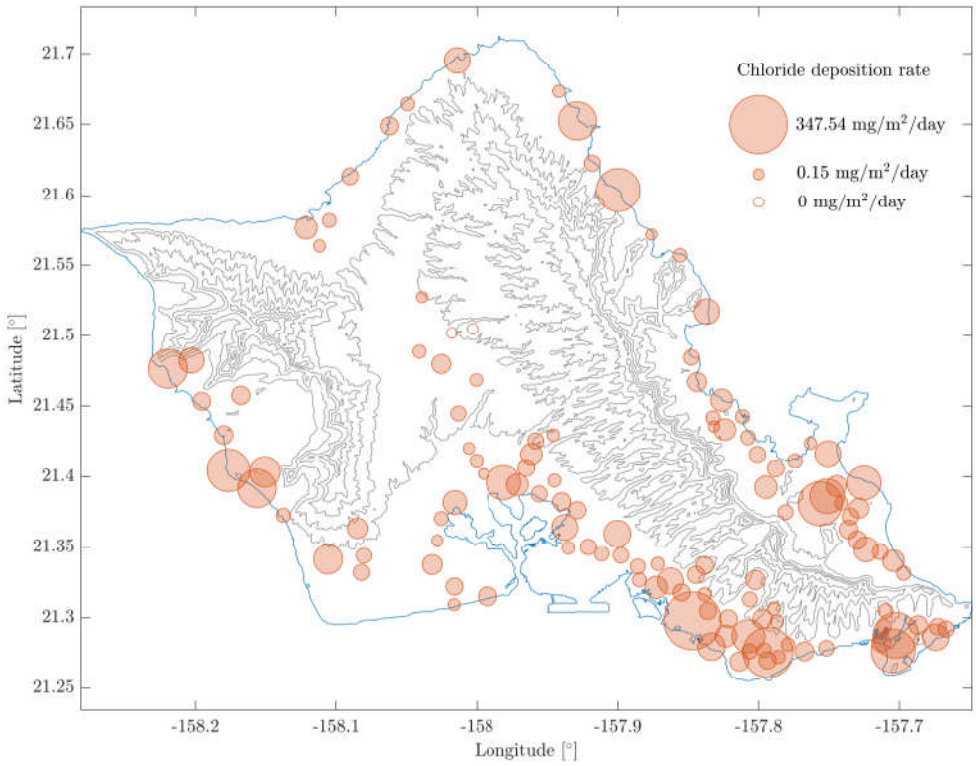

Figure 7. Chloride deposition rates at the testing sites.

can influence its value at small scale (such as the terrain topography and the obstacles due to constructions or trees), not to mention possible measurement errors and uncertainties. It is evident from Figure 7 a general inverse relationship between chloride deposition rate and the shoreline distance. Null or almost zero values of the chloride deposition rate occur in the central part of the island whereas the largest chloride deposition rates are recorded close to the shoreline. High values of the chloride deposition rate occur in the areas close to the windward shoreline, especially in the southeast, and they appear consistent with the prevailing winds (see Figure 4 and Figure 5). Relatively smaller values of the chloride deposition rate occur along the leeward shoreline, and they are mainly attributable to Kona wind (see Figure 5).

It is useful pointing out that some empirical relationships have been proposed to estimate the chloride accumulation at the shoreline given the wave motion characteristics near the coast (e.g. Alcántara et al., 2015; Feliu et al., 2001). These relationships are especially useful for mapping the chloride accumulation inland by means of physics-based models that depend on the deposition rate at the shore (e.g., Meira et al., 2008). Their general form is the following:

$$S_0 = aH^b + c \text{ for } H \geq H_{\min}, \tag{1}$$

where S_0 is the deposition rate at the shoreline and H is a parameter related to the sea wave height whereas $H_{\min}$ is its minimum value. Moreover, a, b and c are regression coefficients. For instance, Feliu et al. (2001) proposed two nonlinear regression models where H is the average sea wave height or its squared value for $c = 0$. Alcántara et al. (2015) adopted a linear regression model ($b = 1$) where H is the average spectral

sea wave height. Considering the average significant sea wave height equal to 1.68 m at the buoy in Kāne'ohe Bay (which is the highest average value recorded among the buoys in Figure 3), the linear regression provided by Alcántara et al. (2015) can be applied by using such value in place of the average spectral sea wave height. In fact, significant and spectral sea wave height are almost equivalent in this case since deep water condition holds (e.g. Vandever et al., 2008), being the depth larger than one-twentieth the wavelength. So doing, a predicted value of the chloride deposition rate on the coast equal to 89.64 mg/m^2/day is obtained, which fairly well agrees with the values of 60.73-112.01 mg/m^2/day recorded at the nearest pertinent testing sites close to the shoreline.

5. Hazard mapping

5.1. Corrosion intensity measure

The definition of the intensity measure plays an important role in hazard assessment. In the present work, the corrosion current density i_{corr} at the reinforcement level is selected as intensity measure to map the chloride-induced corrosion hazard for reinforced concrete structures exposed to marine atmosphere. In general, alternative corrosion intensity measures can be selected, also depending on the intended application of the corrosion hazard map and accounting for a cost-benefit analysis (Rakotovao Ravahatra et al., 2020). However, the use of the corrosion current density is widespread in the long-term assessment of existing structures under chloride ingress (e.g., Chen & Mahadevan, 2008; Choe et al., 2008; Guo et al., 2023; Hájková et al., 2018; Imperatore et al., 2016; Shekhar et al., 2018; Val, 2007; Vu & Stewart, 2000; Zanini et al., 2020). In fact, by virtue of the Faraday's law of electrochemical equivalence, the pit penetration rate $\dot{p}$ in case of chloride-induced pitting corrosion can be readily estimated as follows (e.g., Hájková et al., 2018):

$$\dot{p} = 0.0116 R i_{corr}, \tag{2}$$

where R is the so-called pitting factor. Once a suitable geometrical model is assumed for the pit (e.g., Val, 2007), the corrosion current density i_{corr} in Equation (2) thus allows to estimate the steel reinforcement area demand attributable to pitting corrosion.

In order to estimate the corrosion current density, it is presumed that chloride ingress in concrete can be simulated as diffusion process. Under the assumption of a one-dimensional transport process, thus the Fick' second law of diffusion applies:

$$\frac{\partial C}{\partial t} = \frac{\partial}{\partial x}\left(D\frac{\partial}{\partial x}C\right), \tag{3}$$

where C is the chloride concentration at distance x into the diffusion zone after an exposure time t and D is the diffusion coefficient. Although Fick' second law is widely used to model chloride ingress in the analysis of reinforced concrete structures exposed to airborne chlorides (e.g., Akiyama et al., 2010; Costa & Appleton, 1999; Mustafa & Yusof, 1994; Qu et al., 2021), it should be considered as a phenomenological tool for the estimation of the chloride profile rather than an accurate mathematical model of the physical phenomenon.

The diffusion coefficient is influenced by several concurrent factors. In the present work, it is evaluated in agreement with the study by Papakonstantinou and Shinozuka (2013), where the diffusion coefficient mainly depends on concrete age (e.g., Luping & Nilsson, 1992; Maage et al., 1996; Pack et al., 2010; Thomas & Bamforth, 1999; Yang et al., 2018). Additionally, it is also considered the influence of existing cracks. Therefore, the diffusion coefficient D is calculated as follows:

$$D = D_{\text{ref}} f_t(t) f_\delta(\delta), \tag{4}$$

where D_{ref} is the constant reference diffusion coefficient. The parameter $f_t(t)$ is the corrective factor of the chloride diffusion coefficient that takes into account the concrete age. The corrective factor $f_\delta(\delta)$ accounts for the effects of existing cracks having width equal to δ.

If the age of concrete initially exposed to chloride is equal to the reference age t_{ref}, then the concrete age is $t' = t + t_{\text{ref}}$, and the following relationship is employed for $f_t(t)$ (e.g., Luping & Gulikers, 2007; Maage et al., 1996; Yang et al., 2018):

$$f_t(t) = \left(\frac{t_{\text{ref}}}{t + t_{\text{ref}}} \right)^n \tag{5}$$

where n is the so-called aging factor. Cracks occur unavoidably in most reinforced concrete structures. Experimental evidence show that cracking has modest influence on chloride penetration provided that the maximum crack width is about 0.1 mm (Zhang et al., 2011), whereas larger values dramatically accelerate such process. Chloride penetration into cracked concrete is a complex mechanism, which can deviate significantly from a pure diffusion process in case of very large crack widths. However, if the crack width is not excessive (as it is expected under ordinary serviceability conditions), then chloride ingress into cracked concrete can be still approximated as diffusion process. This simplifying hypothesis has been largely adopted into previous experimental studies, which derived accordingly some suitable corrective factors for the reference chloride diffusion coefficient to account for the effects of cracking (e.g., Kwon et al., 2009; Park et al., 2012; Zhang et al., 2011). These corrective factors usually depend on the crack width only (Kwon et al., 2009), even though the crack density is also expected to play a role in this regard. In the present work, the relationship proposed by Zhang et al. (2011) is employed for $f_\delta(\delta)$:

$$f_\delta(\delta) = \max\{1, 47.18\delta^2 - 8.18\delta + 1\}, \tag{6}$$

which is valid for δ in [mm] and up to a maximum crack width equal to 0.476 mm.

Equation (3) is solved under the assumption of initial chloride concentration in concrete equal to C_0 and a boundary chloride concentration C_s (i.e., chloride concentration at the boundary of the diffusive zone) that varies in time according to a square-root law as $C_s = C_{s0} + k\sqrt{t}$, where C_{s0} and k are two constants. Under these assumptions and setting $\bar{D} = D_{\text{ref}} f_\delta(\delta)$, the semi-analytical solution of Eq. (3) is (Yang

et al., 2018):

$$C = C_0 + C_{s0}\text{erfc}\left(\frac{x}{2\sqrt{\bar{D}F(t)}}\right) + \frac{kx}{2\sqrt{\pi\bar{D}}}\int_0^{F(t)} \frac{\sqrt{F^{-1}(\tau)}}{(F(t)-\tau)^{3/2}}\exp\left(-\frac{x^2}{4\bar{D}(F(t)-\tau)}\right)\mathrm{d}\tau, \tag{7}$$

with

$$F(t) = \frac{t_{\text{ref}}^n}{1-n}\left(\left(1+\frac{t_{\text{ref}}}{t}\right)^{1-n} - \left(\frac{t_{\text{ref}}}{t}\right)^{1-n}\right)t^{1-n}, \tag{8a}$$

$$F^{-1}(\tau) = \left(\frac{1-n}{t_{\text{ref}}^n}\tau + t_{\text{ref}}^{1-n}\right)^{\frac{1}{1-n}} - t_{\text{ref}}. \tag{8b}$$

Several alternative models are available in the existing literature in order to estimate the corrosion current density i_{corr}. The existing proposals can be broadly classified into model-based and data-driven formulations (e.g., Y. Wang et al., 2020; Xia et al., 2022). A critical review has been also presented by Otieno et al. (2011). On the one hand, model-based formulations have a clear electrochemical basis. On the other hand, data-driven formulations are carried out from data through statistical approaches. Hybrid approaches can also be adopted to derive semi-empirical formulations. Model-based and data-driven formulations have their own pros and cons. However, it has been pointed out (e.g., Y. Wang et al., 2020) that data-driven models are nowadays most common for the quantification of the steel corrosion in concrete structures. Recently, a statistical comparative assessment among some alternative empirical models has been performed by Lu et al. (2019) using available experimental data. This set of empirical models also includes a new formulation developed by the same authors, which turned out to be the most accurate among the examined proposals. Such empirical model proposed by Lu et al. (2019) is thus implemented in the present study to estimate i_{corr} in [μA/cm^2]. It reads:

$$i_{corr} = g_{t_{corr}}(t_{corr})\mathrm{e}^{1.23+0.618\ln C_r - \frac{3034}{T g_{RH}(RH)} - 5\cdot 10^{-3}\rho}, \tag{9}$$

where C_r is the chloride content at depth of reinforcement in [kg/m^3], T is the temperature in [K], RH is the relative humidity and t_{corr} is the duration of the corrosion rate in [year]. The parameter ρ is the ohmic resistivity of the concrete in [kΩcm]. The factors $g_{t_{corr}}(t_{corr})$ and $g_{RH}(RH)$ in Equation (9) are defined as $g_{t_{corr}}(t_{corr}) = 1/\sqrt[3]{1+t_{corr}}$ and $g_{RH}(RH) = 2.5 + RH$, respectively.

5.2. Spatial reconstruction of the environmental variables

The elaboration of the corrosion hazard maps requires the numerical values over the study area of the enviromental variables related to exposure conditions involved in Equations (7)-(8) and Equation (9).

Since temperature and relative humidity do not exhibit large seasonal fluctuations throughout the year, average annual values reported in Sub-section 4.2 (see Figure 6) are considered in Equation (9) for estimating the corrosion current density given the chloride concentration in concrete. The boundary chloride condition needed for estimating the chloride concentration in concrete from Equations (7)-(8) is defined according to Meira et al. (2010) based on the chloride deposition rate. This is available as set of discrete values as shown in Sub-section 4.3 (see Figure 7), and thus there is the need of mapping the spatial distribution of the chloride deposition rate over the whole study area. A data-driven approach is primary adopted in the present work for reconstructing the spatial distribution of the chloride deposition rate given the good spatial coverage of the data reported by Suzuki and Robertson (2011) as shown in Figure 7, but a model-based approach is also implemented for comparison.

The adopted data-driven approach to estimate the spatial variation of the chloride deposition rate is a well-established geostatistical method, namely the ordinary kriging (Cressie, 1990; Li & Heap, 2008). In doing so, the available discrete set of chloride deposition rate values in Figure 7 is considered after outlines removal. Kriging model selection and hyperparameters tuning are performed through leave-one-out cross-validation (e.g., Martin & Simpson, 2003). The model-based approach herein implemented relies on the work by Meira et al. (2008). This is a 1D model that aims at simulating the sea-salt transport and deposition in marine atmosphere zones. Accordingly, the chloride deposition rate S in [mg/m^2/day] at a certain distance d from the shoreline is calculated as follows:

$$S = S_0 \mathrm{e}^{\frac{v_{\mathrm{dep0}}}{\alpha h} \mathrm{e}^{-\frac{\alpha d}{v}} - 1}, \tag{10}$$

where v is the wind speed, v_{dep0} is the deposition velocity at the shoreline, α is a coefficient that rules the reduction of the deposition velocity as function of the shoreline distance and h is the height of the considered layer. The model-based reconstruction of the chloride deposition rate for this case-study by means of Equation (10) is likely most biased when average annual wind data are considered. In fact, the analysis of the wind data has demonstrated that, even though there is a prevailing wind condition in the island, the seasonal variation is very large, and the predominant wind pattern can also be reversed in some days as shown in Sub-section 4.2 (see Figure 5). Hence, it is herein proposed an alternative implementation that relies on average daily wind data shown in Sub-section 4.2 (see Figure 4 and Figure 5). In particular, daily wind data are grouped for sectors of the wind direction, assuming a constant sector width equal to 30°. Then, Equation (10) is applied to each sector, assuming v as the average wind speed for the considered sector and d as the distance from the shoreline along the average wind direction for the considered sector. The deposition rate at the shoreline S_0 is assumed constant and equal to the maximum value among the data in Sub-section 4.3 (Figure 7) recorded close to the coast (after outlines removal). The chloride deposition rate S is finally computed as weighted average of the results obtained from all the sectors, where the weights represent the relative frequency of the daily wind data for the considered sector.

5.3. Concrete data and uncertainty quantification

As regards the initial condition and the concrete mixture needed for estimating the chloride concentration in concrete from Equation (3), they are defined in agreement

with Meira et al. (2010) in order to ensure the consistency with all other parameters employed for the analysis. Particularly, the two considered concrete mixtures are those for which Meira et al. (2010) have derived the experimental data adopted in the present study to correlate the chloride deposition rate and the boundary chloride concentration. One considered mixture has cement content and water-to-cement ratio equal to 406 kg/m^3 and 0.50, respectively. Cement content and water-to-cement ratio for the second mixture are 320 kg/m^3 and 0.65, respectively. It is noted that this second mixture is far from being representative of concrete bridges, and it is taken into account only to examine the influence of concrete composition on corrosion hazard. The age of concrete initially exposed to chloride is assumed equal to 28 days. The depth of the diffusion zone up to the reinforcement level is assumed as random variable. According to Dizaj et al. (2021), it is modeled as Normal random variable with mean and coefficient of variation equal to 25 mm and 0.205, respectively (in the present work, it is truncated between 15 mm and 45 mm). Following Konečnỳ and Lehner (2017), crack width is assumed as Normal random variable with mean and coefficient of variation equal to 0.3 mm and 0.17 (in the present work, an upper bound equal to 0.4 mm is considered to comply with the range of validity for Eq. 6). The mean value of the aging factor is assumed equal to 0.275 as estimated by Andrade et al. (2011) for concrete mixtures similar to those considered in the present analysis. Based on the study by X. Wang et al. (2012), the aging factor is modeled as a Normal random variable with a coefficient of variation equal to 0.15 (in the present work, it is truncated between 0.04 and 0.65). The diffusion coefficient at reference conditions is considered as uncertain variable. In agreement with the work by Shafei et al. (2012), the mean value of the diffusion coefficient at reference conditions D_{ref} in [cm^2/year] is calculated as $\log D_{\text{ref}} = -3.9(w/c)^2 + 7.2(w/c) - 2.5$, where w/c is the water-to-cement ratio. Following Zhu et al. (2019), the diffusion coefficient at reference conditions is assumed as Lognormal random variable with coefficient of variation equal to 0.20. Ohmic resistivity and corrosion current density are also assumed as uncertain variables. Ohmic resistivity is modeled as Lognormal random variable with coefficient of variation equal to 0.12 (Papakonstantinou & Shinozuka, 2013). Random samples of the corrosion current density are also generated according to a Lognormal random variable, with a coefficient of variation equal to 0.34 (Papakonstantinou & Shinozuka, 2013). It is understood that all probabilistic models adopted for the uncertain variables are time-independent.

5.4. Probabilistic corrosion hazard maps

The probabilistic corrosion hazard maps here proposed are meant at providing the spatial distribution of the corrosion intensity measure (i.e., corrosion current density) having a given probability of exceedance within an assigned exposure time window for a specific concrete mixture. The following maps are elaborated using standard Monte Carlo simulations considering a probability of exceedance equal to 2% for exposure periods equal to 50 and 100 years (as a term of comparison, it is pointed out that seismic hazard maps of the United States Geological Survey for Hawaii are available with probabilities of exceedance of 10% and 2% in 50 years). A summary of the variables adopted to elaborate the probabilistic corrosion hazard maps is provided in the Appendix. Figure 8 illustrates the mesh adopted to plot the probabilistic corrosion hazard maps for the study area.

Figure 9 shows the probabilistic corrosion hazard maps in terms of corrosion current

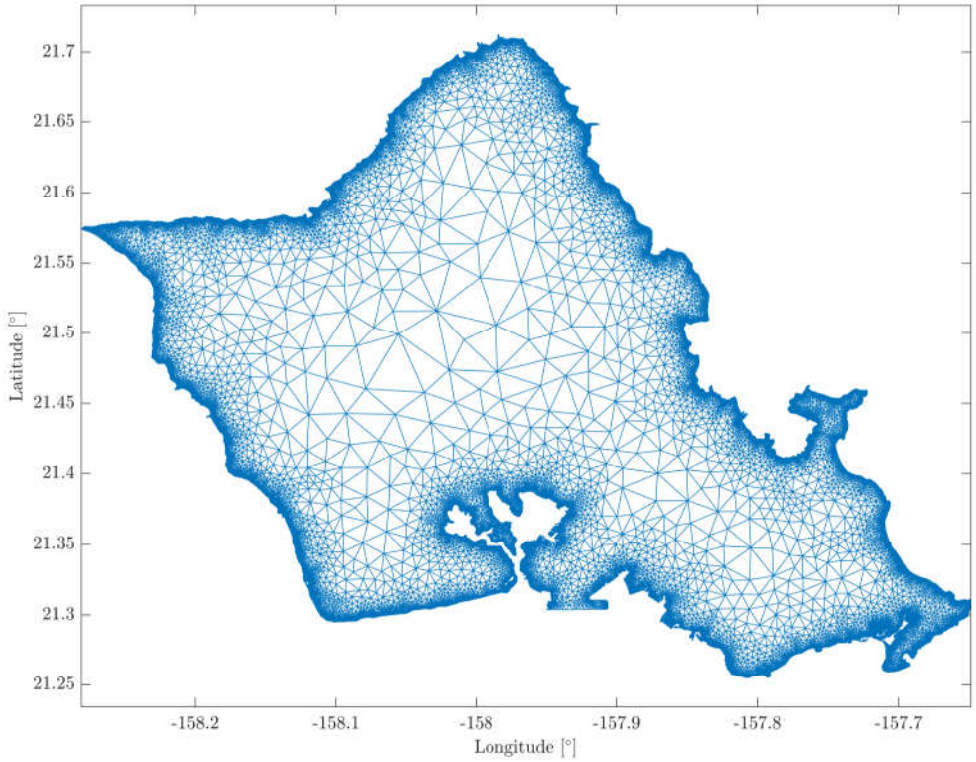

Figure 8. Adopted mesh for the spatial reconstruction of the hazard map.

density for an exposure time window equal to 50 years and 100 years. The maps in Figure 9 are obtained by implementing the data-driven approach for estimating the spatial distribution of the chloride deposition rate (i.e., ordinary kriging). These maps refer to a concrete mixture with cement content and water-to-cement ratio equal to 406 kg/m^3 and 0.50, respectively.

The maximum value of the corrosion current density for an exposure time window equal to 50 years and 100 years is about 0.45 μA/cm^2 and 0.70 μA/cm^2, respectively. For a critical analysis of the results in Figure 9, it is worth recalling that no or negligible corrosion is expected for a corrosion current density lower than 0.1 μA/cm^2. Conversely, corrosion current density values between 0.1 and 0.5 μA/cm^2 correspond to low corrosion intensity, whereas values between 0.5 and 1.0 μA/cm^2 correspond to moderate corrosion intensity and values larger than 1.0 μA/cm^2 correspond to high corrosion intensity (Somerville et al., 1995). For a probability of exceedance equal to 2%, it can be thus noted that a low corrosion hazard level is expected at most for an exposure time window equal to 50 years, while a moderate corrosion hazard level is expected at most for an exposure time window equal to at 100 years. The obtained corrosion hazard maps seem consistent with the presented patterns of the relevant environmental phenomena.

Figure 10 illustrates the absolute value of the difference between the corrosion current density values reported into Figure 9 obtained by means of a data-driven spatial reconstruction of the chloride deposition rate (i.e., ordinary kriging) and the corresponding values estimated through a model-based approach (i.e., Eq. (10) proposed by Meira et al. (2008)). The same concrete composition is assumed, and a probability of exceedance equal to 2% over an exposure time window equal to 100 years is

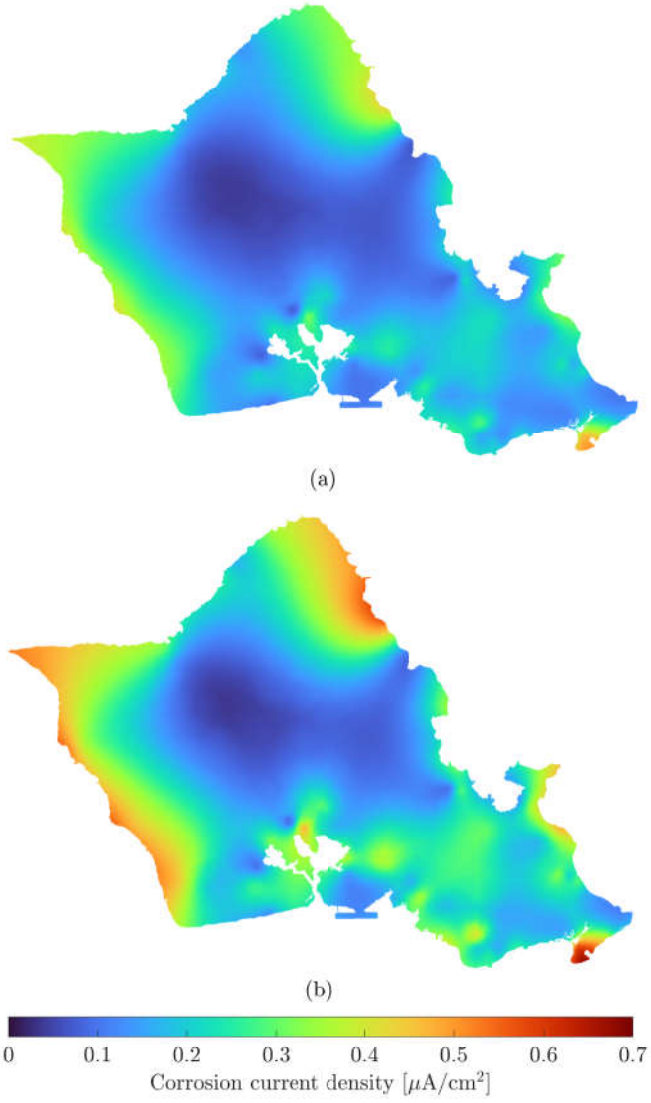

Figure 9. Probabilistic corrosion hazard maps in terms of corrosion current density for an exposure time window equal to 50 years (a) and 100 years (b). The probability of exceedance is 2%, whereas cement content and water-to-cement ratio are equal to 406 kg/m^3 and 0.50, respectively (the data-driven approach is employed to estimate the spatial distribution of the chloride deposition rate).

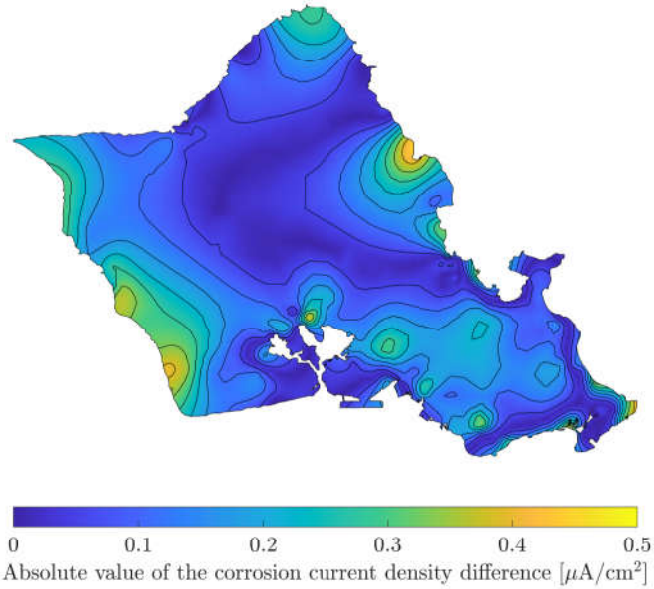

Figure 10. Absolute value of the difference between the results reported in Figure 9 and those obtained by implementing the model-based approach for evaluating the spatial distribution of the chloride deposition rate, given an exposure time window equal to 100 years. The probability of exceedance is 2%, whereas cement content and water-to-cement ratio are equal to 406 kg/m^3 and 0.50, respectively.

considered. Figure 10 thus serves at quantifying the scattering about the estimates of the corrosion current density due to the use of alternative approaches for the evaluation of the spatial distribution of the chloride deposition rate. The relative difference between the data-driven and the model-based approach for the spatial reconstruction of the chloride deposition rate is less than 30% for about 60% of the nodes within the mesh adopted to plot the maps. It can be inferred from Figure 10 that the data-driven and the model-based approach for estimating the spatial distribution of the chloride deposition rate lead to fairly similar predictions of the corrosion hazard in most of the windward areas close to the shoreline (with the possible exception of some narrow zones), and also in most part of the central area of the island, despite the qualitative and quantitative differences between the two approaches. The maximum difference between the two approaches is found on leeward. Here, the corrosion current density values calculated by means of the data-driven prediction of the spatial distribution of the chloride deposition rate are found larger than those estimated using the model-based approach. The large difference on leeward between the two approaches is attributable to the fact that the exposure conditions here deviates significantly from the hypotheses underlying the model-based approach adopted for estimating the spatial distribution of the chloride deposition rate. It should be also considered that the data-driven approach is expected to be less accurate in reconstructing the chloride deposition rate on leeward, given the low number of testing sites in this part of the island.

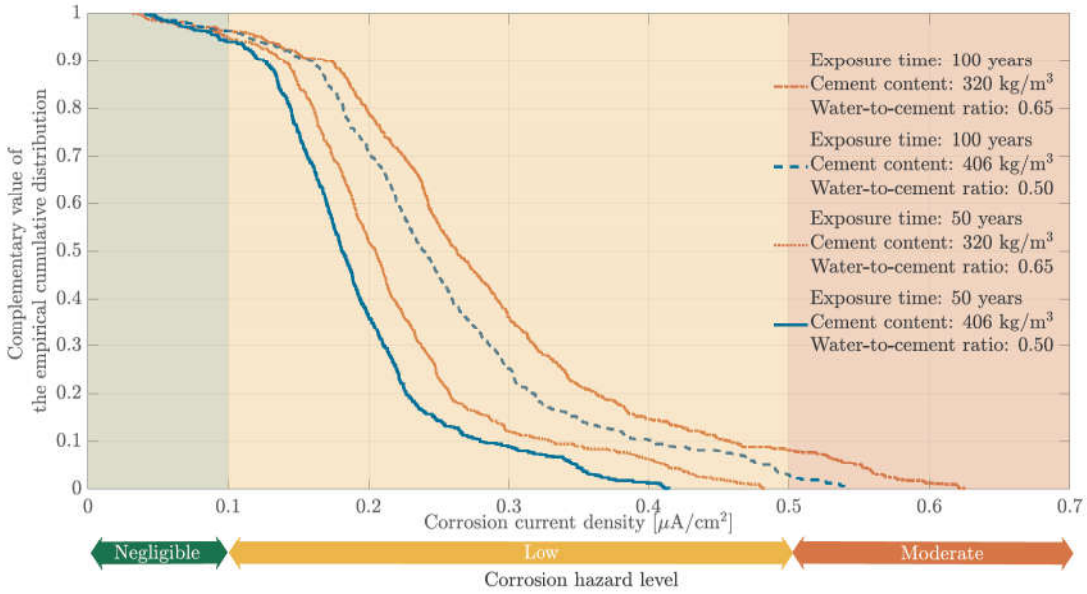

Figure 11. Distribution of the corrosion current density values estimated at the concrete bridge sites for different exposure time windows and concrete mixtures given a probability of exceedance equal to 2%.

6. Sensitivity analysis and correlations

6.1. Sensitivity analysis for concrete mixture and diffusion zone thickness

Figure 11 shows the distribution of the corrosion current density values estimated at concrete bridge sites reported into Sub-section 4.1 (see Figure 2) for different exposure time windows and concrete mixtures, given the probability of exceedance equal to 2% (the data-driven approach is herein employed to estimate the spatial distribution of the chloride deposition rate). The curves in Figure 11 highlight the role of the concrete mixture in ruling the corrosion hazard level, since a low cement content and a large water-to-cement ratio facilitates the corrosion of steel reinforcement. For instance, Figure 11 shows that a moderate corrosion hazard level is predicted in about 3% of the concrete bridge sites (i.e., almost 20 bridge sites) for an exposure time window equal to 100 years considering cement content and water-to-cement ratio equal to 406 kg/m^3 and 0.50, respectively. If cement content and water-to-cement ratio are assumed equal to 320 kg/m^3 and 0.65, respectively, then the concrete bridge sites that exhibit a moderate corrosion hazard level grows up to about 8% (i.e., almost 50 bridge sites).

The influence of the diffusion zone thickness is investigated into Figure 12. A time window equal to 100 years is assumed for this sensitivity analysis, and two mean values of the diffusion zone thickness are considered (namely, 20 mm and 40 mm) while neither the coefficient of variation nor probabilistic distribution have been changed (the data-driven approach is employed once again to estimate the spatial distribution of the chloride deposition rate). Figure 12 shows that the cumulative distribution of the corrosion intensity measure at the concrete bridge sites for a cement content of 406 kg/m^3 and water-to-cement of 0.50 after 100 years is close to that estimated for a cement content of 320 kg/m^3 and water-to-cement of 0.65 if the corresponding mean values of the diffusion zone thickness are equal to 20 mm and 40 mm, respectively. The comparison between Figure 12 and Figure 11 especially highlights the impact

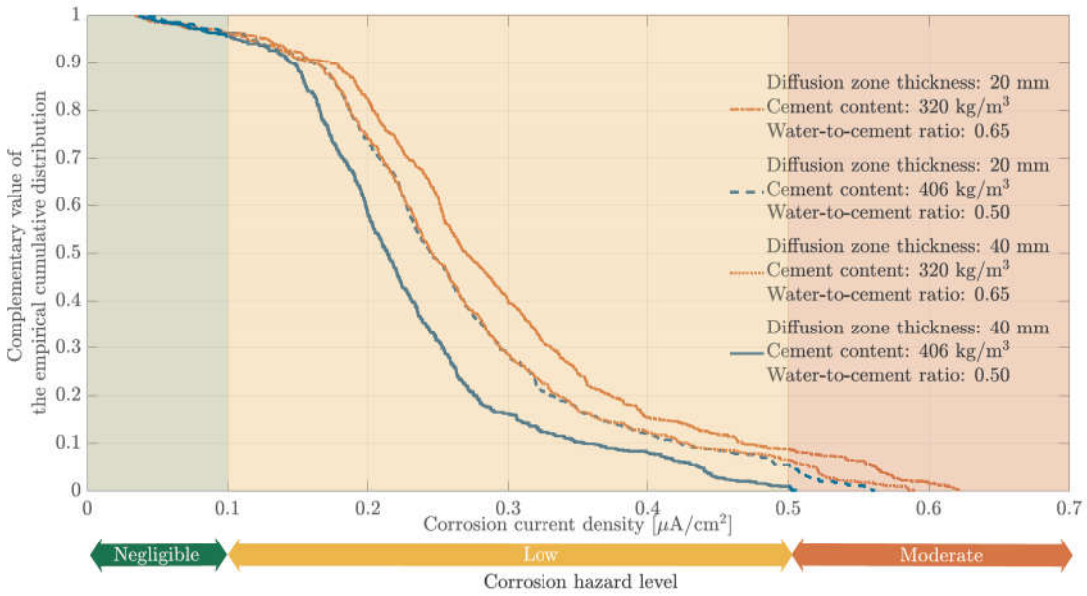

Figure 12. Distribution of the corrosion current density values estimated at the concrete bridge sites for different diffusion zone thicknesses and concrete mixtures given a probability of exceedance equal to 2% (exposure time equal to 100 years).

of the diffusion zone thickness on the corrosion hazard level and, in turn, on bridges management. While a moderate corrosion hazard level has been estimated in about 3% of the concrete bridge sites (i.e., almost 20 bridge sites) for a mean diffusion zone thickness equal to 25 mm considering cement content and water-to-cement ratio equal to 406 kg/m^3 and 0.50, respectively, it turns out to be always low (i.e., corrosion current density less than 0.5 μA/cm^2 given a probability of exceedance equal to 2% and an exposure time of 100 years) if the mean diffusion zone thickness is increased up to 40 mm.

6.2. Correlation between corrosion hazard and actual bridges condition rating

Finally, it is worthy examining how the estimated corrosion hazard correlates with actual bridges condition reported into the National Bridge Inventory for Hawaii (as of December, 2020). The motivation for this correlation analysis is in line with the aim of previous studies by Alogdianakis et al. (2020, 2022), who attempted to deduce impact and existence of patterns between the actual bridges condition and some explanatory variables (including geographical, geometrical, structural and environmental parameters).

The present correlation analysis relies on the simplifying assumptions that corrosion phenomena are mostly responsible for the bridges condition and the lack of previous interventions on them. The corrosion current density is considered to quantify the severity of the corrosion hazard while typical corrosion-induced deterioration phenomena (i.e., section loss, deterioration, cracking, spalling) are taken into account to evaluate the bridges condition. With this premise, Figure 13 illustrates the distribution of the corrosion current density values estimated at concrete bridges sites reported into Sub-section 4.1 (see Figure 2) for a probability of exceedance equal to 50%, in such

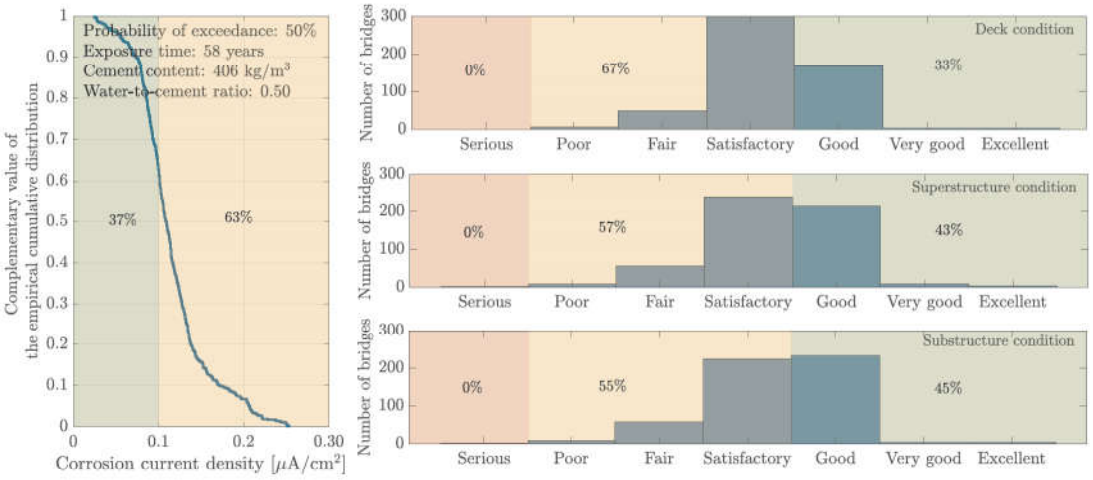

Figure 13. Median distribution of the corrosion current density values estimated at the concrete bridges site (probability of exceedance equal to 50%, 58-years exposure time window), together with actual condition rating.

a way to investigate the correlation between the corrosion levels and actual bridges condition in terms of median value of the corrosion current density (the data-driven approach is herein considered to estimate the spatial distribution of the chloride deposition rate). Since most concrete bridges were built around 60-70ies, a constant exposure time window equal to the average age of concrete bridges is assumed, which is 58 years (referred to 2020). It is considered the concrete mixture with cement content and water-to-cement ratio equal to 406 kg/m^3 and 0.50, respectively, because this composition should be more representative of the actual building material employed in bridges construction than the other mixture considered in the present study. While the study by Alogdianakis et al. (2020) over all United States bridges has required the segmentation of bridges stock data, a much smaller study area is here analyzed, and thus it is reasonable to take into account the entire bridges stock without a preliminary disaggregation. In light of the motivations of the present analysis as well as the uncertainty level, such simplifications and approximations are deemed acceptable to understand whether a correlation exists between the corrosion levels estimated at large scale and the actual bridges condition. In this sense, Figure 13 also shows the actual condition rating for bridge components and sub-assemblies as per the National Bridge Inventory for Hawaii.

According to the present analysis, the corrosion hazard level is null (i.e., corrosion current density less than 0.1 μA/cm^2) or low (i.e., corrosion current density between 0.1 μA/cm^2 and 0.5 μA/cm^2) at the bridges site. This seems in agreement with the actual rating since the number of bridges ranked with serious conditions (i.e., serious loss of section, deterioration or spalling) is almost null and there are no bridges ranked with critical condition (i.e., advanced deterioration) or imminent failure condition. In detail, about 67% of the decks are ranked with poor conditions (i.e., section loss, deterioration or spalling), fair conditions (i.e., minor section loss, cracking or spalling), and satisfactory conditions (i.e., minor deterioration). This evidence seems in satisfactory agreement with the low corrosion level predicted by the present analysis for about 63% of the bridges site. Furthermore, about 33% of the decks are ranked with good, very good or excellent conditions (i.e., minor general problems or none). This evidence fairly well matches with the null corrosion level predicted by the present analysis for

about 37% of the bridges site. A similar correlation can be found if the condition rating of bridge superstructures and substructures are considered. Therefore, despite the inherent limitations and the rather large (aleatory and epistemic) uncertainties involved this analysis, a significant correlation has been found, on average, between the corrosion hazard levels and actual bridges condition.

7. Conclusions

Coastal areas are one of the most urbanized zones on the planet. To figure out their relevance, it is useful to highlight that coastal shoreline counties in United States occupy less than 10% of the whole land, but 39% of the whole population lived in as per 2010, with a 2020 projected population density almost equal to 200 persons/km^2 (excluding Alaska) (NOAA, 2013). Because of the large urbanization of the coastal areas, suitable strategies must be thus implemented to quantify and mitigate the risk at territorial scale in such zones.

Within this framework, the original contribution of the present paper deals with a holistic probabilistic procedure to analyze and map the corrosion hazard at regional scale for reinforced concrete infrastructure in coastal areas exposed to marine atmosphere, with special attention to bridges. It is known that risk management requires information about hazard, exposure, and vulnerability. In this perspective, probabilistic corrosion hazard maps can be a valuable tool for assessing the risk of existing reinforced concrete bridges at territorial scale in coastal regions, and they can be a meaningful decision-making support for planning the interventions required to enhance the resilience of transportation networks in such areas.

The proposed methodology has been applied to estimate the corrosion hazard for reinforced concrete bridges at Oahu Island (Hawaii, United States). Herein, a possible correlation has been found between the predicted corrosion hazard level and available evidences about the actual bridge conditions. Particularly, the predicted current corrosion hazard levels agree with the fair-to-good conditions observed for most of the existing bridges. Considering the current trend of extending the infrastructure lifetime, however, a non negligible number of bridges requires proper attention since they might be subjected to a moderate corrosion hazard in the mid-long term.

It is too evident that the accuracy of the final corrosion hazard estimates depends on the quality of all data and models needed for the simulations. In this regard, the presented procedure can be further improved in such a way to incorporate new data when available, for instance by means of Bayesian updating techniques. The elaboration of different scenarios by taking into account alternative models is also of utmost importance. This is helpful to recognize the influence of models and data on the final hazard estimates. Ultimately, this would also allow to better reflect the existing uncertainties about materials and environmental conditions.

Finally, it is pointed out that the implemented methodology can be adapted for the probabilistic corrosion hazard assessment of reinforced concrete structures located in other coastal regions. The main challenge is related to the availability of data. In fact, data about sea waves, wind, temperature, humidity and rainfall are often available for industrialized countries whereas those about chloride deposition rate are usually few. A model-based approach can be adopted to predict the chloride deposition rate over the considered study area when data are scarce or missing, possibly in combination with corrective factors to account for the elements on the ground that can hinder or facilitate the penetration of chlorides inland.

Appendix

Table 1 provides a summary of the input variables adopted to elaborate the probabilistic corrosion hazard maps.

Table 1. Overview of the input variables adopted to elaborate the probabilistic corrosion hazard maps.

Variable	Type	Note	Sources/References
Daily wind speed and direction	Spatial variable	For model-based reconstruction of the chloride deposition rate	RAWS USA Climate Archive, National Oceanic and Atmospheric Administration
Average annual surface temperature	Spatial variable		(Giambelluca et al., 2014)
Average annual relative humidity	Spatial variable		(Giambelluca et al., 2014)
Chloride deposition rate	Spatial variable	Data-driven prediction of the chloride deposition rate via ordinary kriging	(Suzuki & Robertson, 2011)
		Model-based reconstruction of the chloride deposition rate	(Meira et al., 2008)
Concrete composition	Scalar variable	Cement content equal to 406 kg/m^3, water-to-cement ratio equal to 0.50 (reference mix)	(Meira et al., 2010)
		Cement content equal to 320 kg/m^3, water-to-cement ratio equal to 0.65 (for sensitivity analysis)	
Thickness of the diffusion zone up to the reinforcement level	Scalar variable	Normal random variable with mean and coefficient of variation equal to 25 mm and 0.205, respectively (truncated between 15 mm and 45 mm, reference value)	(Dizaj et al., 2021)
		Normal random variables with mean values equal to 20 mm or 40 mm and coefficient of variation equal to 0.205 (truncated between 15 mm and 45 mm, for sensitivity analysis)	
Crack width	Scalar variable	Normal random variable with mean and coefficient of variation equal to 0.3 mm and 0.17, respectively (truncated up to 0.4 mm)	(Konečný & Lehner, 2017; Park et al., 2012; Zhang et al., 2011)
Aging factor	Scalar variable	Normal random variable with mean and coefficient of variation equal to 0.275 and 0.15, respectively (truncated between 0.04 and 0.65)	(Andrade et al., 2011; X. Wang et al., 2012)
Diffusion coefficient at reference conditions	Scalar variable	Lognormal random variable with empirical model-based calculation of the mean value and coefficient of variation equal to 0.20	(Shafei et al., 2012; Zhu et al., 2019)
Corrosion current density	Scalar variable	Lognormal random variable with empirical model-based calculation of the mean and coefficient of variation equal to 0.34	(Lu et al., 2019; Papakonstantinou & Shinozuka, 2013)

Data availability statement

The data that support the findings of this study have been provided herein or are freely available for download from open repositories.

Disclosure statement

The authors confirm that there are no relevant financial or non-financial competing interests to report.

Acknowledgments

The Authors would like to thank Luca Caracoglia (Northeastern University, United States) for his helpful suggestions about wind data analysis. The Authors would also acknowledge the Reviewers for their useful comments and suggestions.

The work of Giuseppe Quaranta is framed within the RETURN Extended Partnership funded by the European Union Next-GenerationEU (National Recovery and Resilience Plan – NRRP, Mission 4, Component 2, Investment 1.3 – D.D. 1243 2/8/2022, PE0000005). Bruno Briseghella acknowledges the support from the National Natural Science Foundation of China (Grant No. 51778148). Camillo Nuti received partial financial support for the present study through MIUR PRIN 2020 (Grant No. 020P5572N_005).

References

Akiyama, M., Frangopol, D. M., & Yoshida, I. (2010). Time-dependent reliability analysis of existing rc structures in a marine environment using hazard associated with airborne chlorides. *Engineering Structures*, *32*(11), 3768–3779.

Alcántara, J., Chico, B., Díaz, I., De la Fuente, D., & Morcillo, M. (2015). Airborne chloride deposit and its effect on marine atmospheric corrosion of mild steel. *Corrosion Science*, *97*, 74–88.

Alcántara, J., Chico, B., Simancas, J., Díaz, I., Morcillo, M., et al. (2017). Marine atmospheric corrosion of carbon steel: a review. *Materials*, *10*(4), 406.

Alipour, A., & Shafei, B. (2016). Seismic resilience of transportation networks with deteriorating components. *Journal of Structural Engineering*, *142*(8), C4015015.

Alipour, A., Shafei, B., & Shinozuka, M. S. (2013). Capacity loss evaluation of reinforced concrete bridges located in extreme chloride-laden environments. *Structure and Infrastructure Engineering*, *9*(1), 8–27.

Alogdianakis, F., Charmpis, D. C., & Balafas, I. (2020). Macroscopic effect of distance from seacoast on bridge deterioration – Statistical data assessment of structural condition recordings. *Structures*, *27*, 319–329.

Alogdianakis, F., Dimitriou, L., & Charmpis, D. C. (2022). Data-driven recognition and modelling of deterioration patterns in the us national bridge inventory: A genetic algorithm-artificial neural network framework. *Advances in Engineering Software*, *171*, 103148.

Ambler, H., & Bain, A. (1955). Corrosion of metals in the tropics. *Journal of Applied Chemistry*, *5*(9), 437–467.

Andrade, C., Castellote, M., & d'Andrea, R. (2011). Chloride aging factor of concrete measured by means of resistivity. In *Proceedings of the XII international conference on durability of building materials and components*. Porto.

ASCE. (2019). *2019 Hawaii infrastructure report card.*

ASCE. (2021). *2021 American infrastructure report card: Bridges.*

Ataei, N., & Padgett, J. E. (2015). Influential fluid–structure interaction modelling parameters on the response of bridges vulnerable to coastal storms. *Structure and Infrastructure Engineering*, *11*(3), 321–333.

Bastidas-Arteaga, E., Chateauneuf, A., Sánchez-Silva, M., Bressolette, P., & Schoefs, F. (2010). Influence of weather and global warming in chloride ingress into concrete: A stochastic approach. *Structural Safety*, *32*(4), 238–249.

Bastidas-Arteaga, E., Schoefs, F., Stewart, M. G., & Wang, X. (2013). Influence of global warming on durability of corroding rc structures: A probabilistic approach. *Engineering Structures*, *51*, 259–266.

Bertero, R. D., & Bertero, V. V. (2002). Performance-based seismic engineering: the need for a reliable conceptual comprehensive approach. *Earthquake Engineering & Structural Dynamics*, *31*(3), 627–652.

Bourreau, L., Gaillet, L., Bouteiller, V., Schoefs, F., Thauvin, B., Schneider, J., & Naar, S. (2020). Spatial identification of exposure zones of concrete structures exposed to a marine environment with respect to reinforcement corrosion. *Structure and Infrastructure Engineering*, *16*(2), 346–354.

Cady, P. D., & Weyers, R. E. (1992). *Predicting service life of concrete bridge decks subject to reinforcement corrosion.* ASTM International.

Chen, D., & Mahadevan, S. (2008). Chloride-induced reinforcement corrosion and concrete cracking simulation. *Cement and Concrete Composites*, *30*(3), 227–238.

Choe, D.-E., Gardoni, P., Rosowsky, D., & Haukaas, T. (2008). Probabilistic capacity models and seismic fragility estimates for rc columns subject to corrosion. *Reliability Engineering & System Safety*, *93*(3), 383–393.

Ciampoli, M., Petrini, F., & Augusti, G. (2011). Performance-based wind engineering: towards a general procedure. *Structural Safety*, *33*(6), 367–378.

Cole, I., Corrigan, P., & Nguyen, V. H. (2012). Steel corrosion map of Vietnam. *Corrosion science and technology*, *11*(4), 103–107.

Cole, I., Paterson, D. A., & Ganther, W. (2003). Holistic model for atmospheric corrosion Part 1 – theoretical framework for production, transportation and deposition of marine salts. *Corrosion Engineering, Science and Technology*, *38*(2), 129–134.

Contento, A., Xu, H., & Gardoni, P. (2020). Probabilistic formulation for storm surge predictions. *Structure and Infrastructure Engineering*, *16*(4), 547–566.

Corvo, F., Minotas, J., Delgado, J., & Arroyave, C. (2005). Changes in atmospheric corrosion rate caused by chloride ions depending on rain regime. *Corrosion Science*, *47*(4), 883–892.

Costa, A., & Appleton, J. (1999). Chloride penetration into concrete in marine environment—part i: Main parameters affecting chloride penetration. *Materials and Structures*, *32*, 252–259.

Cressie, N. (1990). The origins of kriging. *Mathematical geology*, *22*, 239–252.

Das, S., & Sarkar, K. (2021). Atmospheric corrosivity map for management of steel infrastructure in india using iso dose–response function and gridded data. *ASCE-ASME Journal of Risk and Uncertainty in Engineering Systems, Part A: Civil Engineering*, *7*(1), 04020059.

De Larrard, T., Bastidas-Arteaga, E., Duprat, F., & Schoefs, F. (2014). Effects of climate variations and global warming on the durability of rc structures subjected to carbonation. *Civil Engineering and Environmental Systems*, *31*(2), 153–164.

Dizaj, E. A., Padgett, J. E., & Kashani, M. M. (2021). A Markov chain-based model for structural vulnerability assessmentof corrosion-damaged reinforced concrete bridges. *Philosophical Transactions of the Royal Society A*, *379*(2203), 20200290.

Fakhruddin, B., Kintada, K., & Tilley, L. (2021). Probabilistic tsunami hazard and exposure assessment for the pacific islands-Fiji. *International Journal of Disaster Risk Reduction*, *64*, 102458.

Feliu, S., Morcillo, M., & Chico, B. (1999). Effect of distance from sea on atmospheric corrosion rate. *Corrosion*, *55*(9), 883–891.

Feliu, S., Morcillo, M., & Chico, B. (2001). Effect of state of sea on atmospheric corrosion in coastal zones. *British Corrosion Journal*, *36*(2), 157–160.

Franceschini, L., Vecchi, F., Tondolo, F., Belletti, B., & Montero, J. S. (2022). Mechanical be-

haviour of corroded strands under chloride attack: A new constitutive law. *Construction and Building Materials*, *316*, 125872.

Frangopol, D. M., Lin, K.-Y., & Estes, A. C. (1997). Reliability of reinforced concrete girders under corrosion attack. *Journal of structural Engineering*, *123*(3), 286–297.

Giambelluca, T., Chen, Q., Frazier, A. G., Price, J. P., Chen, Y.-L., Chu, P.-S., ... Delparte, D. M. (2013). Online rainfall atlas of Hawai 'i. *Bulletin of the American Meteorological Society*, *94*(3), 313–316.

Giambelluca, T., Shuai, X., Barnes, M., Alliss, R., Longman, R., Miura, T., ... Businger., A. (2014). *Evapotranspiration of Hawaii* (Final Report 2014). U.S. Army Corps of Engineers – Honolulu District, Commission on Water Resource Management, State of Hawaii.

Goda, K., De Risi, R., De Luca, F., Muhammad, A., Yasuda, T., & Mori, N. (2021). Multi-hazard earthquake-tsunami loss estimation of Kuroshio Town, Kochi Prefecture, Japan considering the Nankai-Tonankai megathrust rupture scenarios. *International Journal of Disaster Risk Reduction*, *54*, 102050.

Grange, S. K. (2014). *Averaging wind speeds and directions* (Tech. Rep. No. doi.org/10.13140/RG.2.1.3349.2006). University of Auckland.

Griffis, L., Patel, V., Muthukumar, S., & Baldava, S. (2013). A framework for performance-based wind engineering. In *Advances in hurricane engineering: Learning from our past* (pp. 1205–1216).

Guerra, J. C., Castañeda, A., Corvo, F., Howland, J. J., & Rodríguez, J. (2019). Atmospheric corrosion of low carbon steel in a coastal zone of Ecuador: Anomalous behavior of chloride deposition versus distance from the sea. *Materials and Corrosion*, *70*(3), 444–460.

Günay, S., & Mosalam, K. M. (2013). Peer performance-based earthquake engineering methodology, revisited. *Journal of Earthquake Engineering*, *17*(6), 829–858.

Guo, H.-Y., Jiang, C., Gu, X.-L., Dong, Y., & Zhang, W.-P. (2023). Time-dependent reliability analysis of reinforced concrete beams considering marine environmental actions. *Engineering Structures*, *288*, 116252.

Hájková, K., Šmilauer, V., Jendele, L., & Červenka, J. (2018). Prediction of reinforcement corrosion due to chloride ingress and its effects on serviceability. *Engineering Structures*, *174*, 768–777.

Imperatore, S., Leonardi, A., & Rinaldi, Z. (2016). Strength decay of RC sections for chloride attack. *International Journal of Structural Integrity*, *7*(2).

Invernizzi, S., Montagnoli, F., & Carpinteri, A. (2022). Very high cycle corrosion fatigue study of the collapsed Polcevera bridge, Italy. *Journal of Bridge Engineering*, *27*(1), 04021102.

Ishibashi, H., Akiyama, M., Frangopol, D. M., Koshimura, S., Kojima, T., & Nanami, K. (2020). Framework for estimating the risk and resilience of road networks with bridges and embankments under both seismic and tsunami hazards. *Structure and Infrastructure Engineering*, *17*(4), 494–514.

Karafagka, S., Fotopoulou, S., & Pitilakis, K. (2018). Analytical tsunami fragility curves for seaport RC buildings and steel light frame warehouses. *Soil Dynamics and Earthquake Engineering*, *112*, 118–137.

Kashani, M. M., Maddocks, J., & Dizaj, E. A. (2019). Residual capacity of corroded reinforced concrete bridge components: State-of-the-art review. *Journal of Bridge Engineering*, *24*(7), 03119001.

Kim, Y., Lim, H., Kim, J., & Park, Y. (2011). Corrosivity of atmospheres in the Korean peninsula. *Corrosion Science and Technology*, *10*(4), 109–117.

Koch, G. H., Brongers, M. P., Thompson, N. G., Virmani, Y. P., & Payer, J. H. (2001). *Corrosion cost and preventive strategies in the United States* (Final Report 1999 - 2001 No. R315-01). Federal Highway Administration.

Konečnỳ, P., & Lehner, P. (2017). Effect of cracking and randomness of inputs on corrosion initiation of reinforced concrete bridge decks exposed to chlorides. *Frattura ed Integrità*

Strutturale, *39*, 29–37.

Kurtz, N., Song, J., & Gardoni, P. (2016). Seismic reliability analysis of deteriorating representative US West Coast bridge transportation networks. *Journal of Structural Engineering*, *142*(8), C4015010.

Kwon, S. J., Na, U. J., Park, S. S., & Jung, S. H. (2009). Service life prediction of concrete wharves with early-aged crack: Probabilistic approach for chloride diffusion. *Structural Safety*, *31*(1), 75–83.

Lee, W. K., & Billington, S. L. (2009). *Simulation and performance-based earthquake engineering assessment of self-centering post-tensioned concrete bridge systems* (PEER Report No. 2009/109). Pacific Earthquake Engineering Research Center.

Li, J., & Heap, A. D. (2008). A review of spatial interpolation methods for environmental scientists.

Lu, Z.-H., Lun, P.-Y., Li, W., Luo, Z., Li, Y., & Liu, P. (2019). Empirical model of corrosion rate for steel reinforced concrete structures in chloride-laden environments. *Advances in Structural Engineering*, *22*(1), 223–239.

Luping, T., & Gulikers, J. (2007). On the mathematics of time-dependent apparent chloride diffusion coefficient in concrete. *Cement and concrete research*, *37*(4), 589–595.

Luping, T., & Nilsson, L.-O. (1992). Chloride diffusivity in high strength concrete at different ages. *NORDIC CONCRETE RESEARCH. PUBLICATION NO 11*.

Maage, M., Helland, S., Poulsen, E., Vennesland, O., & Carl, J. E. (1996). Service life prediction of existing concrete structures exposed to marine environment. *Materials Journal*, *93*(6), 602–608.

Martin, J. D., & Simpson, T. W. (2003). A study on the use of kriging models to approximate deterministic computer models. In *International design engineering technical conferences and computers and information in engineering conference* (Vol. 37009, pp. 567–576).

Meira, G. R., Andrade, C., Alonso, C., Borba Jr, J., & Padilha Jr, M. (2010). Durability of concrete structures in marine atmosphere zones – the use of chloride deposition rate on the wet candle as an environmental indicator. *Cement and Concrete Composites*, *32*(6), 427–435.

Meira, G. R., Andrade, C., Alonso, C., Padaratz, I., & Borba, J. (2008). Modelling sea-salt transport and deposition in marine atmosphere zone – a tool for corrosion studies. *Corrosion Science*, *50*(9), 2724–2731.

Mustafa, M., & Yusof, K. (1994). Atmospheric chloride penetration into concrete in semitropical marine environment. *Cement and Concrete Research*, *24*(4), 661–670.

NOAA, U. C. B. (2013). National coastal population report – population trends from 1970 to 2020 [Computer software manual].

Nuti, C., Briseghella, B., Chen, A., Lavorato, D., Iori, T., & Vanzi, I. (2020). Relevant outcomes from the history of Polcevera viaduct in Genova, from design to nowadays failure. *Journal of Civil Structural Health Monitoring*, *10*(1), 87–107.

Otieno, M., Beushausen, H., & Alexander, M. (2011). Prediction of corrosion rate in rc structures-a critical review. In *Modelling of corroding concrete structures: Proceedings of the joint fib-rilem workshop held in madrid, spain, 22–23 november 2010* (pp. 15–37).

Pack, S.-W., Jung, M.-S., Song, H.-W., Kim, S.-H., & Ann, K. Y. (2010). Prediction of time dependent chloride transport in concrete structures exposed to a marine environment. *Cement and Concrete Research*, *40*(2), 302–312.

Padgett, J. E., Spiller, A., & Arnold, C. (2012). Statistical analysis of coastal bridge vulnerability based on empirical evidence from hurricane katrina. *Structure and infrastructure engineering*, *8*(6), 595–605.

Papakonstantinou, K. G., & Shinozuka, M. (2013). Probabilistic model for steel corrosion in reinforced concrete structures of large dimensions considering crack effects. *Engineering Structures*, *57*, 306–326.

Park, S.-S., Kwon, S.-J., & Jung, S. H. (2012). Analysis technique for chloride penetration in cracked concrete using equivalent diffusion and permeation. *Construction and Building Materials*, *29*, 183–192.

Pelle, A., Briseghella, B., Bergami, A. V., Fiorentino, G., Giaccu, G. F., Lavorato, D., ... Nuti, C. (2022). Time-dependent cyclic behavior of reinforced concrete bridge columns under chlorides-induced corrosion and rebars buckling. *Structural Concrete*, *23*(1), 81–103.

Pelle, A., Briseghella, B., Fiorentino, G., Giaccu, G. F., Lavorato, D., Quaranta, G., ... Nuti, C. (2023). Repair of reinforced concrete bridge columns subjected to chloride-induced corrosion with ultra-high performance fiber reinforced concrete. *Structural Concrete*, *24*(1), 332–344.

Pham, N. D., Kuriyama, Y., Kasai, N., Okazaki, S., Suzuki, K., & Nguyen, D. T. (2019). A new analysis of wind on chloride deposition for long-term aerosol chloride deposition monitoring with weekly sampling frequency. *Atmospheric Environment*, *198*, 46–54.

Pongsaksawad, W., Klomjit, P., Khamsuk, P., Sorachot, S., Pälsson, N. S., & Viyanit, E. (2021). Chloride distribution model and corrosion map of structural steels for tropical climate in Thailand. *Science of The Total Environment*, *787*, 147465.

Porter, K. A. (2003). An overview of peer's performance-based earthquake engineering methodology. In *Proceedings of ninth international conference on applications of statistics and probability in civil engineering* (pp. 1–8).

Poston, R. W., & West, J. S. (2005). Investigation of the Charlotte Motor Speedway bridge collapse. In *Structures congress 2005: Metropolis and beyond* (pp. 1–11).

Qeshta, I. M., Hashemi, M. J., Gravina, R., & Setunge, S. (2019). Review of resilience assessment of coastal bridges to extreme wave-induced loads. *Engineering Structures*, *185*, 332–352.

Qu, F., Li, W., Dong, W., Tam, V. W., & Yu, T. (2021). Durability deterioration of concrete under marine environment from material to structure: A critical review. *Journal of Building Engineering*, *35*, 102074.

Rakotovao Ravahatra, N., de Larrard, T., Duprat, F., Bastidas-Arteaga, E., & Schoefs, F. (2020). A cost-benefit methodology for selecting analytical reinforced concrete corrosion onset models. *Advances in Civil Engineering*, *2020*.

Reis, C., Baptista, M. A., Lopes, M., Oliveira, C. S., & Clain, S. (2022). Cascade earthquake and tsunami hazard assessment: A deterministic perspective for engineering purposes. *International Journal of Disaster Risk Reduction*, *75*, 102952.

Saler, E., Donà, M., Pernechele, V., Tecchio, G., & da Porto, F. (2023). Characterisation of an urban bridge portfolio and multi-risk prioritisation accounting for deterioration and seismic vulnerability. *International Journal of Disaster Risk Reduction*, 103596.

Schexnayder, C., Alarcón, L. F., Antillo, E. D., Morales, B. C., & Lopez, M. (2014). Observations on bridge performance during the Chilean earthquake of 2010. *Journal of Construction Engineering and Management*, *140*(4), B4013001.

Shafei, B., Alipour, A., & Shinozuka, M. (2012). Prediction of corrosion initiation in reinforced concrete members subjected to environmental stressors: A finite-element framework. *Cement and Concrete Research*, *42*(2), 365–376.

Shekhar, S., Ghosh, J., & Padgett, J. E. (2018). Seismic life-cycle cost analysis of ageing highway bridges under chloride exposure conditions: Modelling and recommendations. *Structure and Infrastructure Engineering*, *14*(7), 941–966.

Snaiki, R., Wu, T., Whittaker, A. S., & Atkinson, J. F. (2020). Hurricane wind and storm surge effects on coastal bridges under a changing climate. *Transportation research record*, *2674*(6), 23–32.

Somerville, G., Andrade, C., Fagerlund, G., Lagerblad, B., Rodriguez, J., & Tuutti, K. (1995). *The residual service life of reinforced concrete structures* (Final Report No. BRUE-CT92-0591). European Union.

Spence, S. M., & Arunachalam, S. (2022). Performance-based wind engineering: Background and state of the art. *Frontiers in Built Environment*, *8*, 830207.

Stewart, M. G., Wang, X., & Nguyen, M. N. (2011). Climate change impact and risks of concrete infrastructure deterioration. *Engineering Structures*, *33*(4), 1326–1337.

Suzuki, K., & Robertson, I. N. (2011). *Atmospheric chloride deposition rate for corrosion prediction on Oahu* (Research Report UHM/CEE/11-02). State of Hawaii Department of

Transportation Harbors Division, U.S. Department of Transportation Federal Highway Administration.

Thomas, M. D., & Bamforth, P. B. (1999). Modelling chloride diffusion in concrete: Effect of fly ash and slag. *Cement and concrete research*, *29*(4), 487–495.

ANSI/ASHRAE. (2013). *ANSI/ASHRAE standard 169–2013 – Climatic data for building design standards* (Standard 169). American Society of Heating, Refrigerating and Air-Conditioning Engineers, American National Standards Institute.

ISO. (2012). *Corrosion of metals and alloys - corrosivity of atmospheres - classification, determination and estimation* (ISO 9223:2012). International Organization for Standardization.

Val, D. V. (2007). Deterioration of strength of RC beams due to corrosion and its influence on beam reliability. *Journal of Structural Engineering*, *133*(9), 1297–1306.

Vandever, J. P., Siegel, E. M., Brubaker, J. M., & Friedrichs, C. T. (2008). Influence of spectral width on wave height parameter estimates in coastal environments. *Journal of waterway, port, coastal, and ocean engineering*, *134*(3), 187–194.

Vereecken, E., Botte, W., Lombaert, G., & Caspeele, R. (2021). Assessment of corroded prestressed and posttensioned concrete structures: A review. *Structural Concrete*, *22*(5), 2556–2580.

Vu, K. A. T., & Stewart, M. G. (2000). Structural reliability of concrete bridges including improved chloride-induced corrosion models. *Structural safety*, *22*(4), 313–333.

Wang, X., Stewart, M. G., & Nguyen, M. (2012). Impact of climate change on corrosion and damage to concrete infrastructure in Australia. *Climatic change*, *110*(3), 941–957.

Wang, Y., Liu, C., Wang, Y., Li, Q., & Yan, B. (2020). Semi-empirical prediction model of chloride-induced corrosion rate in uncracked reinforced concrete exposed to a marine environment. *Electrochimica Acta*, *331*, 135376.

Xia, J., Shen, J., Li, T., & Jin, W.-L. (2022). Corrosion prediction models for steel bars in chloride-contaminated concrete: A review. *Magazine of Concrete Research*, *74*(3), 123–142.

Yang, L., Ma, Q., & Yu, B. (2018). Analytical solution and experimental validation for dual time-dependent chloride diffusion in concrete. *Construction and Building Materials*, *161*, 676–686.

Zanini, M. A., Faleschini, F., & Pellegrino, C. (2017). Probabilistic seismic risk forecasting of aging bridge networks. *Engineering Structures*, *136*, 219–232.

Zanini, M. A., Toska, K., Faleschini, F., & Pellegrino, C. (2020). Seismic reliability of reinforced concrete bridges subject to environmental deterioration and strengthened with frcm composites. *Soil Dynamics and Earthquake Engineering*, *136*, 106224.

Zhang, S.-f., Lu, C.-h., & Liu, R.-g. (2011). Experimental determination of chloride penetration in cracked concrete beams. *Procedia Engineering*, *24*, 380–384.

Zhu, X., Zi, G., Sun, L., & You, I. (2019). A simplified probabilistic model for the combined action of carbonation and chloride ingress. *Magazine of Concrete Research*, *71*(7), 327–340.